A Seismic Reflection Analysis in the San Francisco Volcano Field, AZ

Austin Hoyle
GEOL394 – April 25th, 2022
Dr. Nicholas Schmerr – Dr. Vedran Lekic

Table of Contents

1 Abstracts

1.1 Plain Text Abstract

The San Francisco Volcano Field (SFVF) is located in northern Arizona, covers more than 4800 square kilometers, and contains over 600 volcanoes. This region shares geological characteristics with the volcanic fields on the Moon and Mars, making it an important site for scientific study. In fact, the National Aeronautics and Space Administration (NASA) has used the area to train astronauts and test prototype equipment. The present study conducted a seismic reflection analysis using data from two seismic lines to explore the geological structure of the subsurface. The aim was to detect two faults located beneath the lava flows surrounding a cinder cone volcano, Volcanic Vent V5704, in the SFVF. The goal of this study is similar to what NASA may have in the future when investigating the Moon and Mars, and the methods used in this report could be useful for addressing these goals. Initially, this report produced two images of the subsurface to the north and south of V5704, but because the lava flows in the area prevent seismic wave energy from traveling far, the results were inconclusive. However, as a follow-on analysis this report showed that varying wave amplitudes along each seismic line provided evidence that the topmost lava rock layer at the surface experiences a sudden vertical thickening in the middle of each line. Since the two faults in question resulted in the bedrock beneath the lava layer to subside vertically about 40 meters between them, this thickening of the topmost layer is consistent with the lava flowing into this subsided portion between the faults.

1.2 Scientific Abstract

The San Francisco Volcano Field (SFVF) is situated on the southern margins of the Colorado Plateau in Northern Arizona. This volcanic structure covers over 4800 square kilometers and is home to over 600 cinder cone volcanoes, most of which are basaltic in composition. The physical and chemical similarities the SFVF shares with the volcano fields on the moon and Mars has prompted scientists to use the site as an analog, and it has been a popular location chosen by the National Aeronautics and Space Association (NASA) to train astronauts and test equipment. That analog work has aided researchers in identifying the various products from common volcanic eruptions, identifying magma sources beneath the surface, and developing a timeline of the geologic history of the area. Past research in the SFVF has established that the volcanic cones align along preexisting faults in the region, specifically the Mesa Butte Fault System (MBFS). However, the existence of these faults in subsurface below the volcanic structures has not yet been confirmed. The objective of this study is to investigate two faults, which form SP Graben in the MBFS, to determine their subsurface structure and determine if their contribution to the volcanic structure above is possible. Understanding mechanisms at which magma travels through the Earth's crust allows for a better understanding of the subsurface structure, as well as provides better understanding of the geological past and future. This objective is similar to the scientific missions we may have on the moon and Mars in the future, and the present study aims to be just one of many steps towards determining best practices for conducting such research in space. This investigation has utilized data from two active source seismic lines that were

deployed in strategic locations on the north and south sides of the basaltic cinder cone volcano vent, V5704, to detect the MBFS beneath the volcano. The data have been processed in a seven-step reflection seismic processing approach, which is covered in detail in the Methods section. The resulting zero-offset reflectivity structure of both seismic lines resulted in incoherent reflectivity likely due to large amounts of seismic wave attenuation in the area. As a result, no direct geological interpretations could be confidently made. However, when comparing the amplitude of arriving waves in various locations along each line, it becomes clear there is a portion on each seismic line that display lower amplitude waves than expected. The lateral inconsistencies in amplitude are likely made possible by the high attenuating basaltic lava flow at the surface suddenly increasing in thickness. This provides evidence for the presence of SP Graben at both research sites, which would increase the depth to the bottom of the lava flow layer and increase overall wave attenuation as observed in the data.

2 Introduction

2.1 Geological History

Between its positioning on the Colorado Plateau and its volcanic history, the San Francisco Volcano Field (SFVF) has been a popular spot for geologists in the past. Covering approximately 4800 square kilometers, the SFVF is home to over 600 volcanic cones (Priest et al., 2001). To understand why the SFVF developed in this way, it is important to know the geological history of the Colorado Plateau. The plateau, which originated during the Precambrian Era, has a metamorphic basement that has been subject to igneous intrusions since its creation. During the Paleozoic and Mesozoic Eras, when the plateau was near sea level, a thick layer of sedimentary rock was deposited above the metamorphic basement (Bell, 2021).

As the Tertiary Period began, the Plateau began its phase of uplift and resulted in the two-kilometer rise in elevation that is seen today (Flowers, 2010). This uplift led to the creation of several fault systems such as the Mesa Butte Fault System (MBFS), the Bright Angel Fault System, the Cataract Fault System, and the Oak Creek Fault System (Mickus and Durrani, 1996). This seismic analysis focuses on two faults within the MBFS, Fault A and Fault B (Figure 1A), located near SP Crater, which is a remnant crater from a basaltic cinder cone volcano. It has been suggested it erupted approximately 70 ka and resulted in the lava flow spilling out to the north, but though some estimates suggest the eruption event occurred 5.5-6 ka (Rittenour et al., 2012).

Following the uplift of the Colorado Plateau, near the end of the Tertiary Period, a wave of volcanism swept through the region due to the complete subduction of the Farallon Plate under the North American Plate (Van der Lee, Nolet, 1997). This period of volcanism deposited layers of lava flows at the surface, with the most recent eruption occurring roughly 1000 ka at Sunset Crater (Mickus and Durrani, 1996). Knowing the geological structure of the area is essential when performing a geophysical seismic survey, as it provides a better understanding of the SFVF's recent evolution.

2.2 Research Objectives and Hypotheses

Previous research within the San Francisco volcanic field (SFVF) has shown that there appears to be preferential alignment of volcanic activity along preexisting faults within the MBFS (Tanaka et al., 1986). If these faults continued under the ancient lava flow that buries them, it's possible that they could be underneath the volcanos in the region (Figure 1). These faults could have acted as a pathway for lava coming to the surface. This is similar to the mechanisms that may have formed the volcano fields that are the subject of a study completed by Le Corvec et al. (2013), which focused on the mechanisms that formed 37 volcano fields and determined that all but one volcano field formed in preferential alignments due to pre-existing faults (the mechanism of interest for this study), tectonic stress level, magma pressure, or a combination of these (Le Corvec et al., 2013).

To determine if these pre-existing faults contributed to the development of the volcanic structures near SP Crater in the SFVF, this study employed a seismic reflection analysis to determine if these faults are present underneath volcanic vent V5704, which

is a basaltic cinder cone volcano near SP Crater and located directly above the potential location of the faults (Bell, 2021). These faults are last observed at the surface approximately 2 km north of volcanic vent V5704, and 1.5 km north to northwest of SP Crater (Figure 1). Southern portions of these faults are buried underneath an ancient lava flow, preventing any visual evidence of the faults being present near volcanic vent V5704.

Seismic data from seismic lines 1A and 1B (Figure 1) have been used to probe the subsurface for the presence of these faults. They have been strategically positioned to straddle volcanic vent V5704 and perpendicular to the proposed fault locations. Each fault displays a vertical displacement of approximately 15-40 meters depending on location (Billingsley et al., 2007), which is expected to stay consistent as the faults continue south.

The hypotheses for this study are as follows:

H_1: SP Graben has southward continuation beyond volcanic vent V5704.

H_2: SP Graben does not have a southward continuation beyond volcanic vent V5704.

If the faults are determined to not be a suitable mechanism for the formation of the local volcanic cone and vents (i.e., this analysis confirms *H_2*), there are still other mechanisms that may cause the preferential alignment outlined above (Le Corvec et al., 2013). Another alternative could be that the lava intruded as a dike through the subsurface geology to reach the surface.

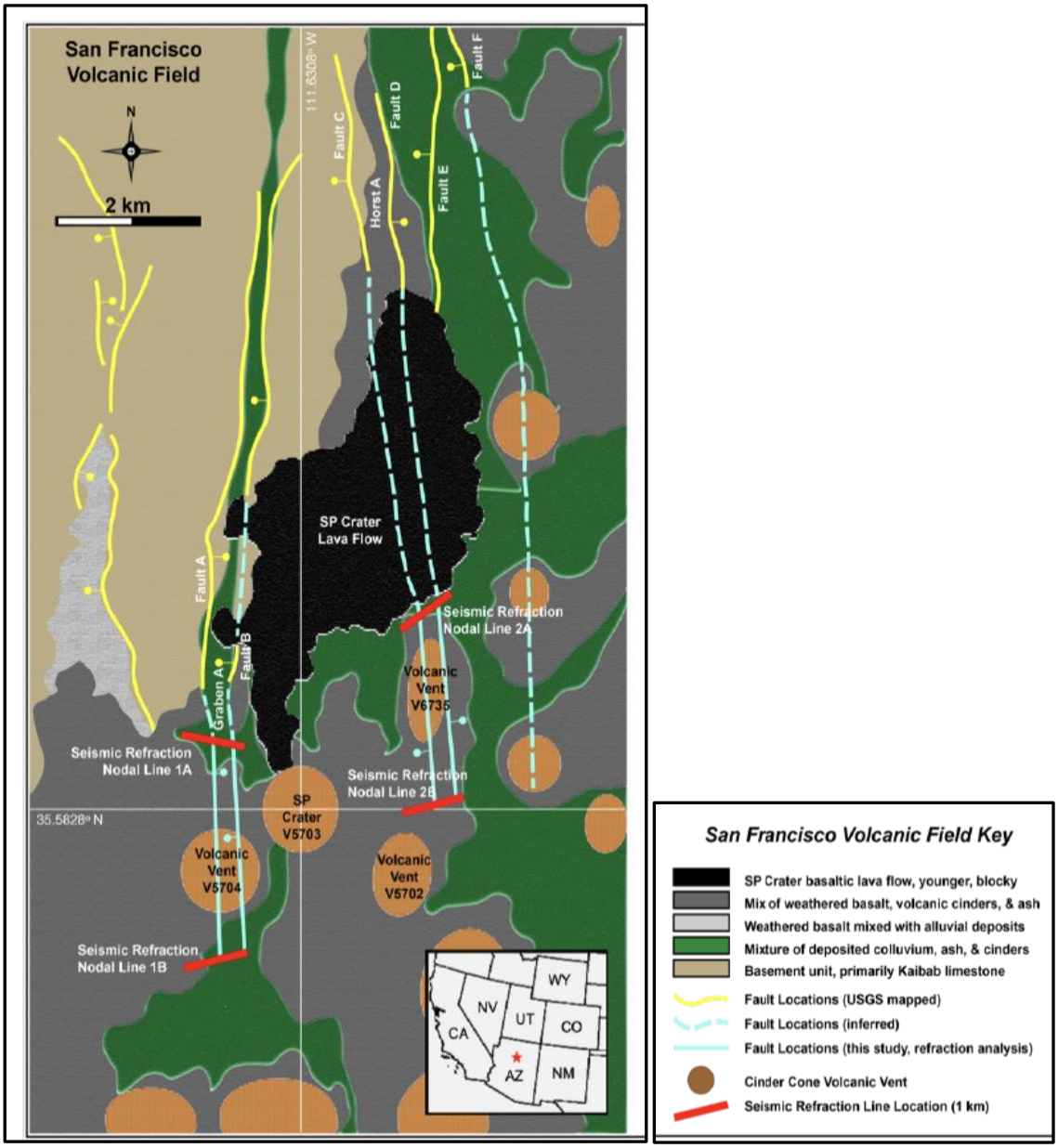

Figure 1: Map of the region of the SFVF near SP Crater, indicating the rock types at the surface. The yellow lines indicate positioning of faults that are visible at the surface, and blue lines indicate the positioning of the proposed continuation of those faults. Red lines indicate where nodal lines were placed during the data collection phase. Figure from Bell (2021).

3 Background

3.1 Geophysics Overview

To begin addressing the hypotheses, a seismic survey was utilized to probe the subsurface geology. A seismic survey consists of a few key pieces of equipment, the first being an active source, responsible for creating a disturbance at the surface to send kinetic energy in all directions in the form of waves. While surface waves are typically low frequency and high amplitude, this study focused on the higher frequency lower amplitude body waves that travel through and collects data on the subsurface. These waves propagate in the shape of a sphere in all directions, but its simpler to think of them as vectors that travel the most direct path from the source, interacting with the subsurface geology, and back to the surface as shown in Figure 2. The active source can be anything from a hammer blow on a metal plate, to an explosion triggered at the surface. This energy travels in a number of different types of body waves, but the type of body waves this study will focus on are the type that reflect off of interfaces below the surface. These interfaces are contacts between two different rock layers that have different geophysical properties. When the seismic wave strikes an interface, some energy reflects and travels back to the surface, while the rest of the energy continues through to the next layer below, to later possibly reflect off of another interface (Figure 2).

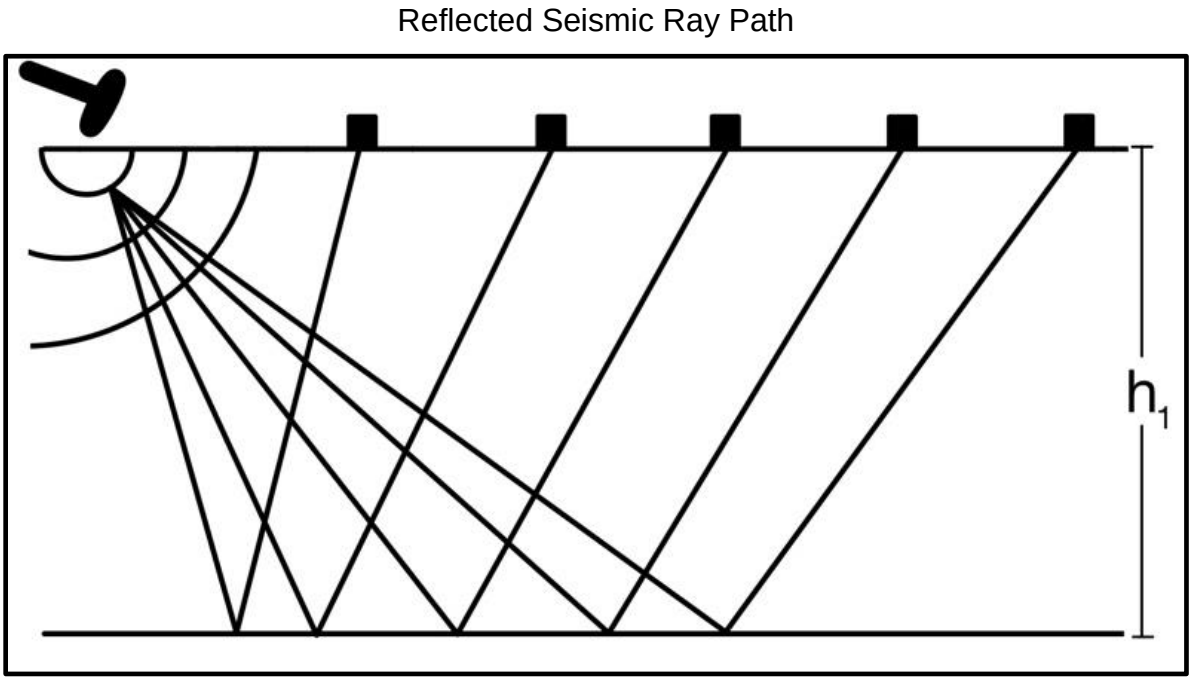

Figure 2: A simplified rendering of a seismic survey. Seismic rays travel from an active source, travel down to an interface at a depth h_1, and reflect back to the surface for a measuring device to record the resulting ground motion.

When the seismic waves reach the surface after a reflection and generate ground motion, a geophone captures this motion in discrete time intervals. Specifically, the geophone measures a voltage created within the geophone from relative vertical movement between a magnet and a coil. The varying arrival times of the reflected waves,

when paired with other important known variables such as the distance the geophone is from the source or the seismic velocity of the layers below, make it possible to reconstruct an image of geologic features under the surface which is the goal for this analysis.

The data that will be utilized for this analysis have been collected by Dr. Ernie Bell, a former PhD student with the University of Maryland, and were used to perform a seismic *refraction* analysis of the subsurface geology. A seismic refraction analysis is different in the sense that refracted waves *bend* through the subsurface when interreacting with interfaces, rather than reflect. This typically provides a much shallower view into the subsurface.

The equipment used for data collection included similar equipment as laid out above. The active source chosen was what is known as a Propelled Energy Generator (PEG). This is a vehicle mounted slingshot that cranks a 40 kg cylindrical pole against the resistance of an elastic band, and when triggered is shot rapidly toward a ½ inch thick, two ft by two ft metal plate fashioned on the ground. This provides seismic waves that propagate energy with a frequency range of 10 Hz to 250 Hz (R.T. Clark Geophysical Equipment Co., 2014).

The measuring device chosen for data acquisition is what is known as Fairfield ZLand 3C 5 Hz Nodal seismometers (Zsystems Zland 1C and 3C Node User Manual, 2014). These are similar to the geophones explained above with the additional advantage that they can record ground motion in all three dimensions rather than just the vertical dimensions. The two seismic lines that were laid out each consisted of 51 individual nodes, spaced at 20-meter intervals. This provided a seismic line of approximately one kilometer. After the nodes where in place, 10 shots were executed at each of the 32 shot locations chosen (Figure 3). This provided a total of 320 shots and 16,320 individual measurements for each seismic line (Bell 2021).

Site Location and Nodal - Source Geometry

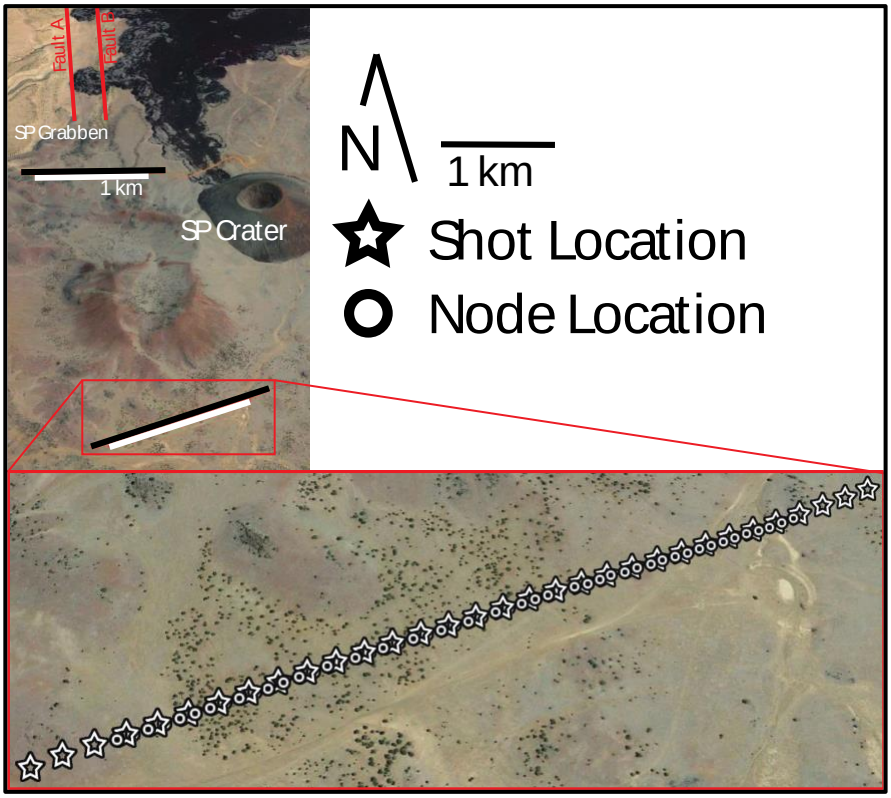

Figure 3: Google Earth image of the site location and indicates source a node geometry. Each line had the same geometry.

3.2 Previous Research

In the seismic refraction analysis performed by Bell (2021), unexpected wave attenuation produced inconclusive results by limiting the study's reliability and data collection. The results were only reliable up to 40 meters of depth for seismic line 1A and 10 meters of depth for seismic line 1B. The refraction study aimed to resolve faults at greater depths, but the high wave attenuation produced results similar to as if there were a series of shorter nodal lines that were set up in sequence, offering only a shallow depiction of the subsurface geology.

Despite the inconclusiveness of the seismic refraction study, it still provided some valuable information that will aid in the efforts for this study. Using a 2-D velocity profile (Figure 4, panel A), it was determined that for seismic line 1A, there appears to be two seismic velocities present, one at 800 m/s and the other near 2500 m/s. The first of which is the basaltic lava bed and the second is believed to be the Kaibab Limestone exposed at the surface in the north. The 2-D velocity profile for seismic line 1B was only able to resolve the lava bed indicating the depth to the basalt/ limestone interface has increased from approximately 40 meters at seismic line 1A to approximately 80 meters at seismic line 1B (Bell, 2021). Knowing the general structure of the layers beneath the surface has aided the present analysis in processing the data.

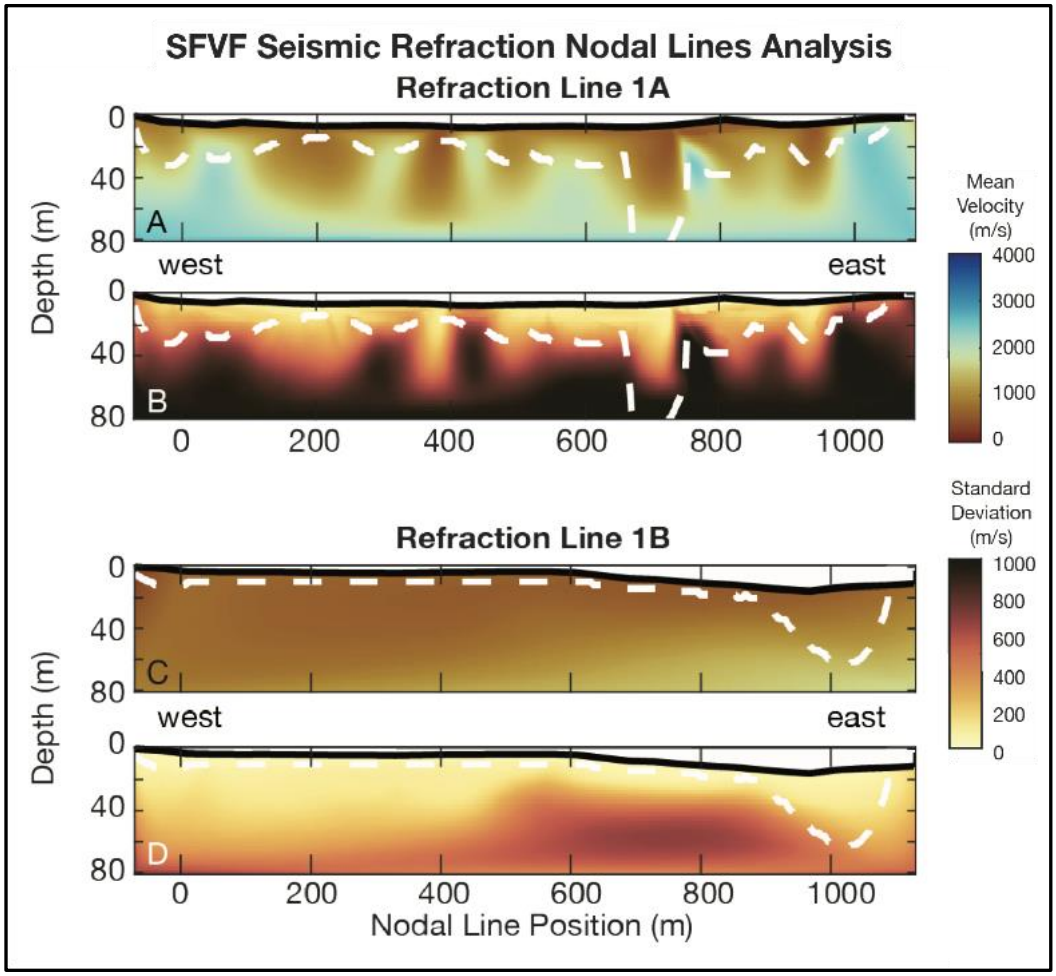

Figure 4: Results from the 2D inversion for the SFVF refraction surveys completed in 2021. The mean P-wave velocity of the ensemble is shown in A and C, while the standard deviation of the ensemble is shown in B and D for each refraction line respectively. The white dashed line indicates the deepest modelled penetration of the seismic rays recorded by the nodes. Velocity scale is the same for the two velocity panels, and the two standard deviation panels as indicated by the color bars. Standard deviation determined by model misfit and variability, when fitting simulation iterations to real data. (Bell, 2021).

3.3 Terrestrial Analog Relevance

The SFVF and similar volcano fields have been used as analogs to the surface of other terrestrial bodies within our solar system due to the similarities these places share (Romig et al., 2007; Tanaka et al., 2009; Bell, 2021). These analog sites provide researchers the ability to study geological structures with similar geophysical traits to those found on the moon or Mars. Developing proper experiment design on terrestrial analogs is and has been a vital part of NASA's goals to explore the moon. For the Apollo missions, NASA has provided their astronauts with proper training in field geology techniques including sampling, geological mapping and observing, and geophysical methods so they could be well equipped to carry out these missions on the moon. (NASA, 1996; NASA, 1970).

The Apollo missions NASA completed on the moon have provided the scientific community valuable data and information on the surface and shallow subsurface of the moon (NASA, 1976), and the preparations for these missions here on earth aided the

success of these missions. NASA has continued to use the SFVF as an analog environment over the past five decades with one of the more recent training missions being the NASA Desert Research and Technology Studies (RATS) expedition, in which a lunar rover mission was conducted that spanned the course of several weeks (Gruener et al., 2013). The success of future missions to the moon and Mars depends on conducting thorough scientific research in analogous environments like the SFVF. This study aims to improve our understanding of the best practices for conducting a seismic reflection analysis in these extraterrestrial settings.

4 Methods

To perform the analysis in this study, a MATLAB script created by Dr. Nicholas Schmerr and refined and customized by myself has been employed. The process for the seismic reflection analysis utilizes various programed functions from the CREWES software package, which is a series of MATLAB scripts (Version 2101; Margrave, 2019) that can be called on and used from the main script. The raw data that act as the input for this MATLAB script are a discrete timeseries intervaled at 0.5 milliseconds, or 2,000 Hz (Bell, 2021), measuring ground motion in the x, y, and z directions.

4.1 Processing Steps

This analysis utilized a seven-step process to transform the raw data into a final result. This process includes:

1. Cutting and resampling seismic data
2. Common midpoint gathering (CMP)
3. Frequency filtering
4. Polarization filtering
5. Normalizing seismic traces
6. Phase Muting
7. Normal moveout correction (NMO)

This section will serve to elaborate the specifics of each step, providing visual examples when necessary.

4.1.1 Cutting and Resampling Seismic Data

The raw data received in the SEG2 format was originally sampled in the 2000 Hz native to the measuring equipment. The traces spanned 10 seconds each, providing 20,000 measurements for every trace. Given that there were two seismic lines, 32 shot locations at each line, 10 shots occurring at each shot location, and 51 measuring devices recording 20,000 measurements for each shot, some culling of unnecessary data was necessary to provide feasibility in computational time.

To accomplish this, each of the over 32,000 traces were cut to 2 seconds in length. Given that the target reflection should be occurring at approximately 40-80 meters in depth and accounting for a p-wave velocity of 800 m/s, the most immediate reflection should arrive at the nearest receiver in approximately 0.1 seconds, and the furthest receiver should record it in approximately 1.6 seconds. Each trace was also resampled

by removing every other measurement in the data to lower the sampling rate down to 1000 Hz. As a general rule of thumb for resampling, one must maintain at least four times the source frequency, so as to not remove important seismic data. In section 4.1.3, it will be shown that the maximum frequency this analysis will focus on is 200 Hz. Setting our sampling frequency to 1000 Hz allows this study plenty of flexibility to ensure the important information is retained in the data. These two steps effectively shrunk the data set from both lines from having over 652 million measurements, to having approximately 65 million measurements while maintaining the capabilities to address the hypotheses.

4.1.2 Common Midpoint Gathering (CMP)

Each seismic trace represents a unique pairing of a source and receiver and depending on the distance between this pairing, one can gather together all the traces that would have the same reflection point in the subsurface. In Figure 5A, there are seven different pairings all centered around the same reflection point. Each seismic path gets longer as the separation grows between the pair, but the reflection point stays the same. Before processing the data, every trace is grouped together based on a common midpoint, in groups that can be visualized by Figure 5B. In reality, reflections rarely line up at the exact same point as depicted in Figure 5. Rather, this reflection “point” is a bin that groups together traces that have a reflection point within this bin. This group will remain together for the rest of the processing steps, until they undergo a normal move out correction to account for the varying arrival times of the same reflection point. This correction will essentially collapse these traces into a single trace. This will be explained more in detail in the NMO section.

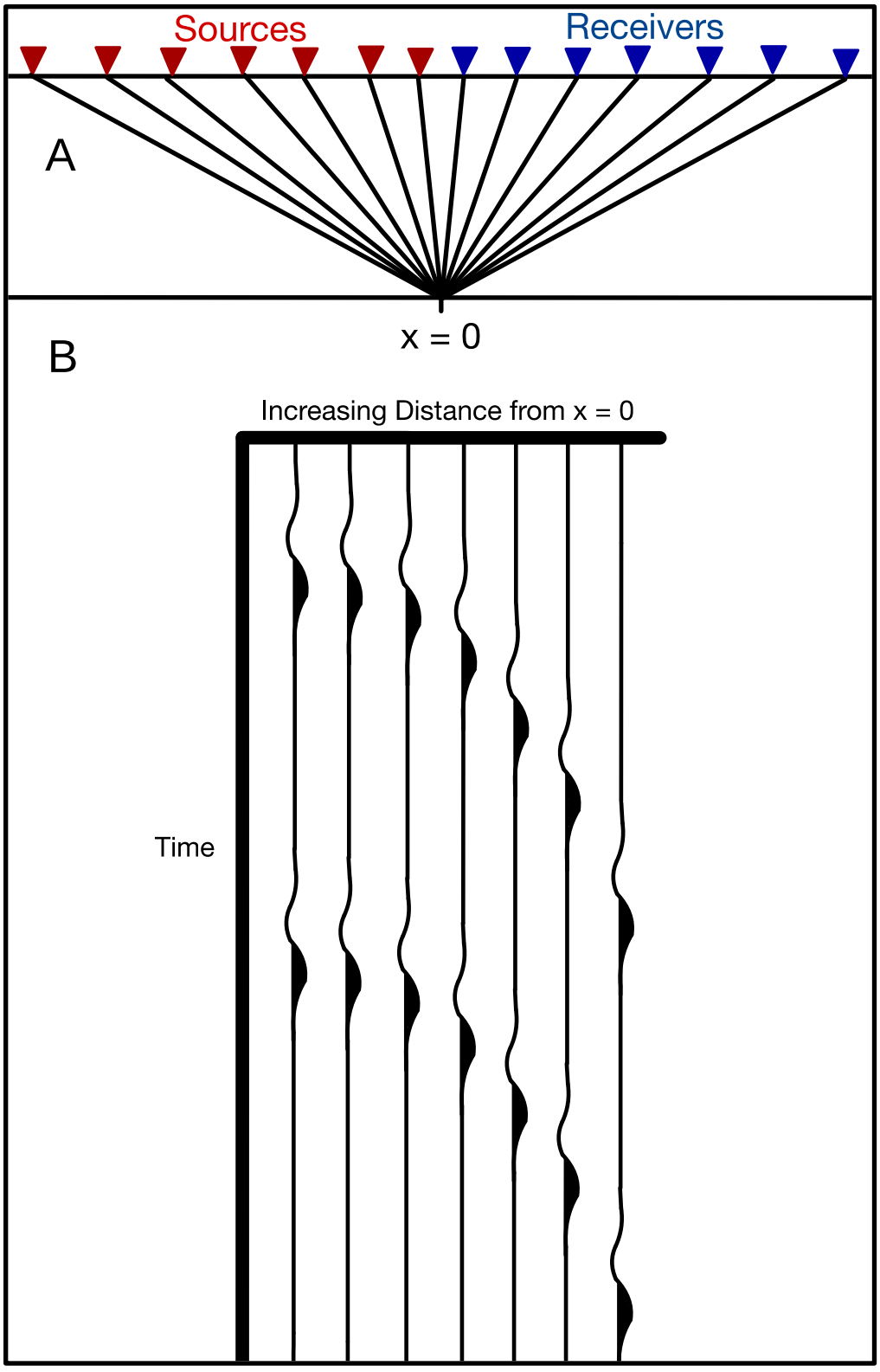

Figure 5: Simplified illustration depicting seismic rays that share a common midpoint. The traces corresponding to each receiver and source pairing can be shown in panel B

4.1.3 Frequency Filtering

The original seismic traces contain waves that come from a multitude of different sources other than our active source, all of which are generally referred to as noise. This noise has a wide range of frequencies that can be removed by applying a frequency filter. The active source, PEG, has a natural frequency at which it will create seismic waves, and to determine this frequency I executed a spectral analysis. This analysis produced a spectrogram which shows what frequencies are strongest in magnitude for each receiver. In Figure 6A, an example is shown for shot group 11. There is an area of high intensity frequencies occurring centered at station number 16, which is a result of the PEG over saturating the data. As distance from the source increases, two bands of high intensity frequency bands remain. One occurs near the 30 Hz range and can be attributed to the surface waves that are not of interest to the present study. The higher frequency waves are the lower amplitude body waves that are important for this investigation.

Reformatting the data shown in Figure 6B allows for a better selection of frequency limits for the filter that was applied to the data. Ignoring the lower frequency surface waves indicated by the red line in Figure 6B, the target range of frequencies are near the 50-200 Hz range. This was later adjusted to 70-200 Hz range as the polarization analysis that will be covered next provided evidence of higher frequency surface wave persisting in our original bandpass. Figure 8A and 8B (next section) displays the input and output of this filter. This example comes from the same shot group indicated in Figure 6, shot group 11. A butterworth bandpass filter of order 4 was applied to the data, effectively removing all waves from our data that exhibit frequencies outside of the 70-200 Hz range, therefore improving the frequency to noise ratio.

Spectral Analysis

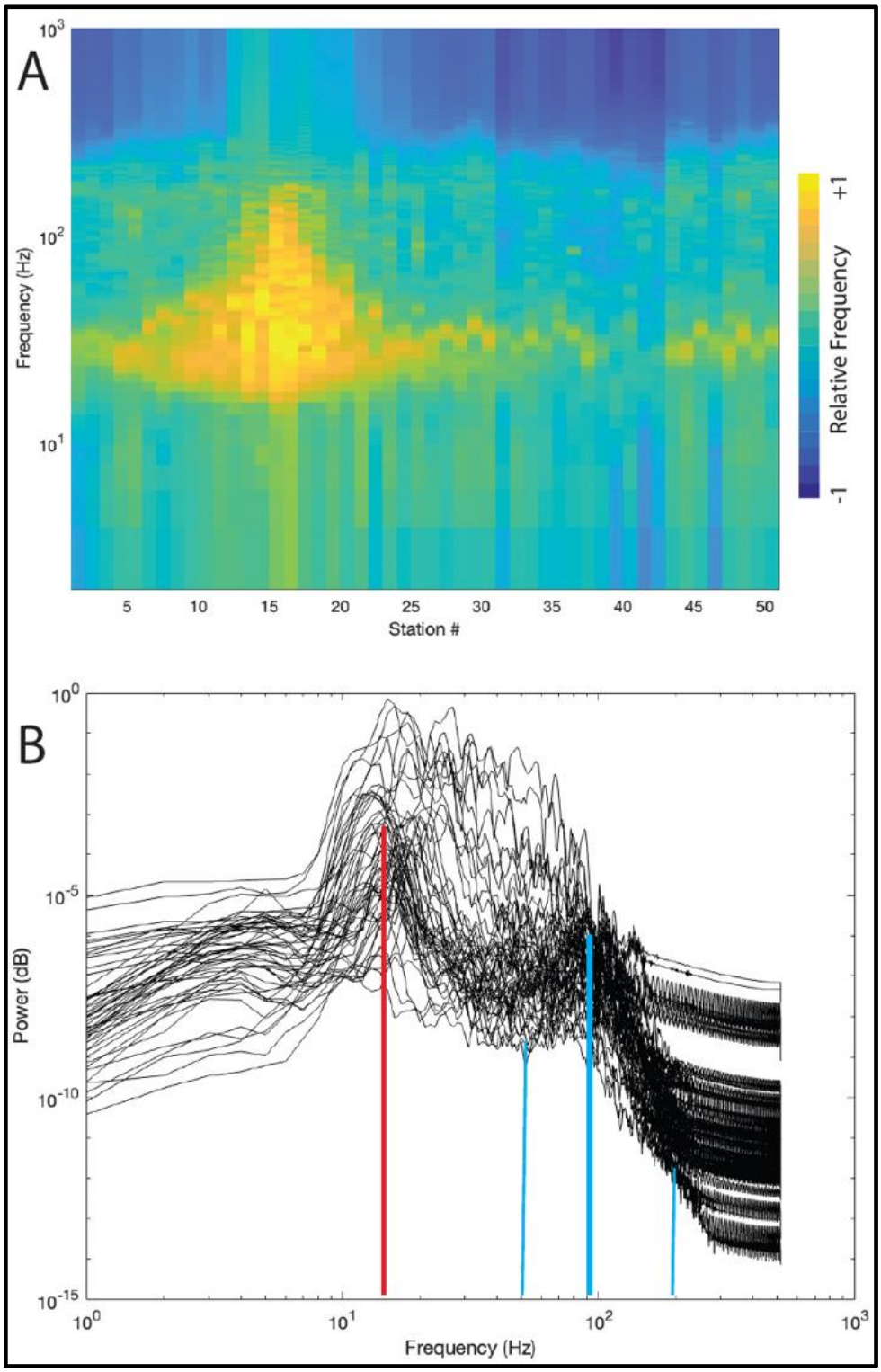

Figure 6: Results from the spectral analysis performed to determine the limits for the bandpass filter applied to the data. A) A Frequency (y-axis) vs Station Number (x-axis) example, with the color map expressing power intensity. B) A Power (y-axis) vs Frequency (x-axis) example with each trace representing a different node. Red line indicates the peak that should be ignored, blue lines indicate the peak of interest.

4.1.4 Polarization Filtering

When a receiver measures ground motion it is essentially measuring the particle motion of an incoming wave. Given that this data was recorded in three directions, there is effectively a record of the particle motion of each wave in three-dimensional space. It is known that our target waves, reflected p-waves, are polarized in a direction that is a combination of the z direction and the direction parallel to the seismic line. Random noise or any remaining surface waves intended to be suppressed are typically randomly polarized or polarized differently from the p-waves. Taking advantage of this, the polarization filter applied to the data can determine the polarity of our seismic traces and project the particle motion onto a new polarized axis.

The process begins by taking the three corresponding traces of each direction, x y z, and begins moving along each trace set in specified time windows. Within each time window, how much the particle motion varies along a given axis is computed and stored in a variable called the variance $Var[N]$. The covariance is then calculated along each axis pairing, which is similar to the variance but between two components. The covariance is stored in $Cov[X,Z]$ (Montalbetti & Kanasewich, 1970). These values are put together into a data matrix called the covariance matrix that effectively shows how much the particle is moving in each direction for this time window. The format of the covariance matrix is:

$$\begin{matrix} Var[X] & Cov[X,Y] & Cov[X,Z] \\ Cov[X,Y] & Var[Y] & Cov[Y,Z] \\ Cov[X,Z] & Cov[Y,Z] & Var[Z] \end{matrix}$$

The computation of the eigenvectors (also called the principal axes) is used to determine the polarity of the particle motion for this time window. The eigenvector that has the largest associated eigenvalue provides us with a new axis at which the particle motion is the axis at which particle motion is *most* polarized (Montalbetti & Kanasewich, 1970). The particle motion is then projected onto this new axis, which retains particle motion information along the new axis, while suppressing particle motion information that is not. Figure 7 shows a simplified step by step process on a 2-D system to help better visualize and understand the process. This process is the largest contributor to the increase in signal to noise ration throughout all processing steps. Again, using shot group 11, Figure 8B and 8C indicates the input and output of the polarization filter. This filter is successful at further suppressing the surface wave energy and greatly reducing background noise.

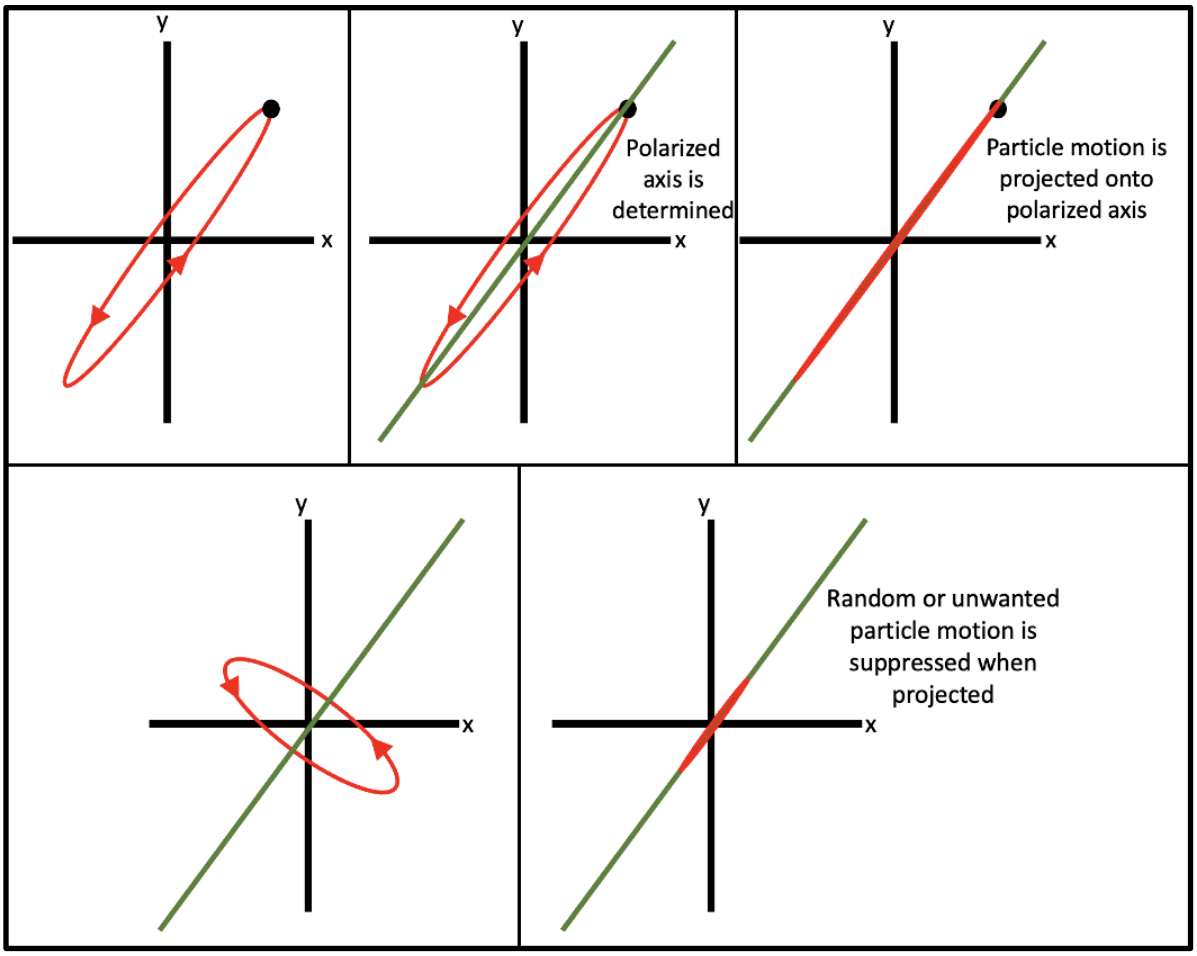

Figure 7: Simplified illustration of the processes outlined in section 4.1.4, showing the suppressing of oppositely or randomly polarized wave motion.

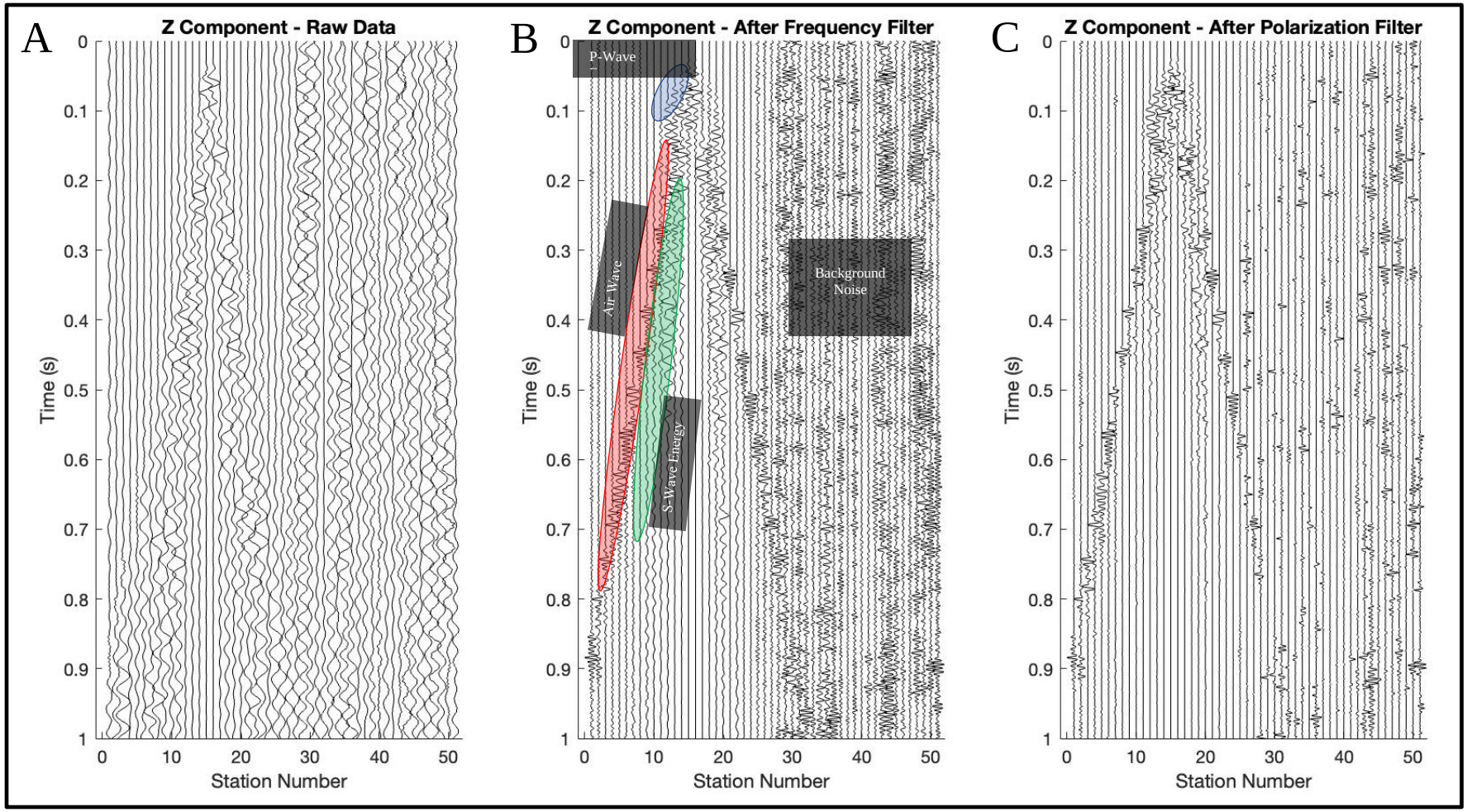

Figure 8: Shot gather traces from shot group 11 depicting the different filtering steps. Panel A indicates the Z component before any processing has been executed. Panel B indicates the same data after a frequency bandpass filter with limits of 70Hz to 200 Hz has been applied to it. Various types of waves in the data have been highlighted and labelled. Panel C shows the final result after frequency and polarization filtering has been complete.

4.1.5 Normalizing Seismic Traces

The maximum amplitude recorded within each seismic trace is stored into a variable. Every other measurement within that trace is then divided by the maximum value to normalize the entire trace to a value of ± 1. This is to ensure that each trace when plotted in the final result are on the same scale. It is important to note when examining Figure 8, which has been normalized for visualization, you may notice that the traces recording ground motion further from the source appear to have more noise recorded. However, due to the high wave attenuation in the area, very little seismic energy is arriving at these stations. Therefore, the maximum values recorded in these traces are on the same scale as inherent background noise. For the traces that *are* receiving seismic energy, when divided by the high amplitude value of the seismic waves, the noise seemingly gets reduced. This result can actually be used as a confirmation the frequency filtering and polarization filtering is successful at reducing background noise.

4.1.6 Phase Muting

The phase muting step is used to remove waves that have well-defined velocities. For example, the high frequency wave indicated with the red shaded region on Figure 9A is what is known as the air wave. The airwave was not completely removed after the frequency and polarization filters, and it would be beneficial to remove this wave. The p-wave velocity of air is well defined at 343 m/s providing a velocity window of 300 m/s to 400 m/s. This process finds the point in time that each of these velocities should reach the measuring device. All values are set to zero between these intersections effectively removing the wave from the data (Figure 9B).

4.1.7 Normal Moveout Correction (NMO)

The normal moveout step adjusts the traces in each CMP gather along the time axis to allow the reflections to align properly in time. The traces are then collapsed into a single trace through stacking of amplitudes (Figure 10). The stacking adds additional signal to noise ratio improvement, given that consistent waves throughout each trace will increase in amplitude, whereas random noise with decrease. This single trace represents the reflectivity structure in a straight line from its common midpoint location to the surface. When these newly collapsed traces are displayed in series from the beginning to end of the seismic line, the amplitudes of seismic waves provide a 2-D image of the reflectivity structure beneath the seismic line.

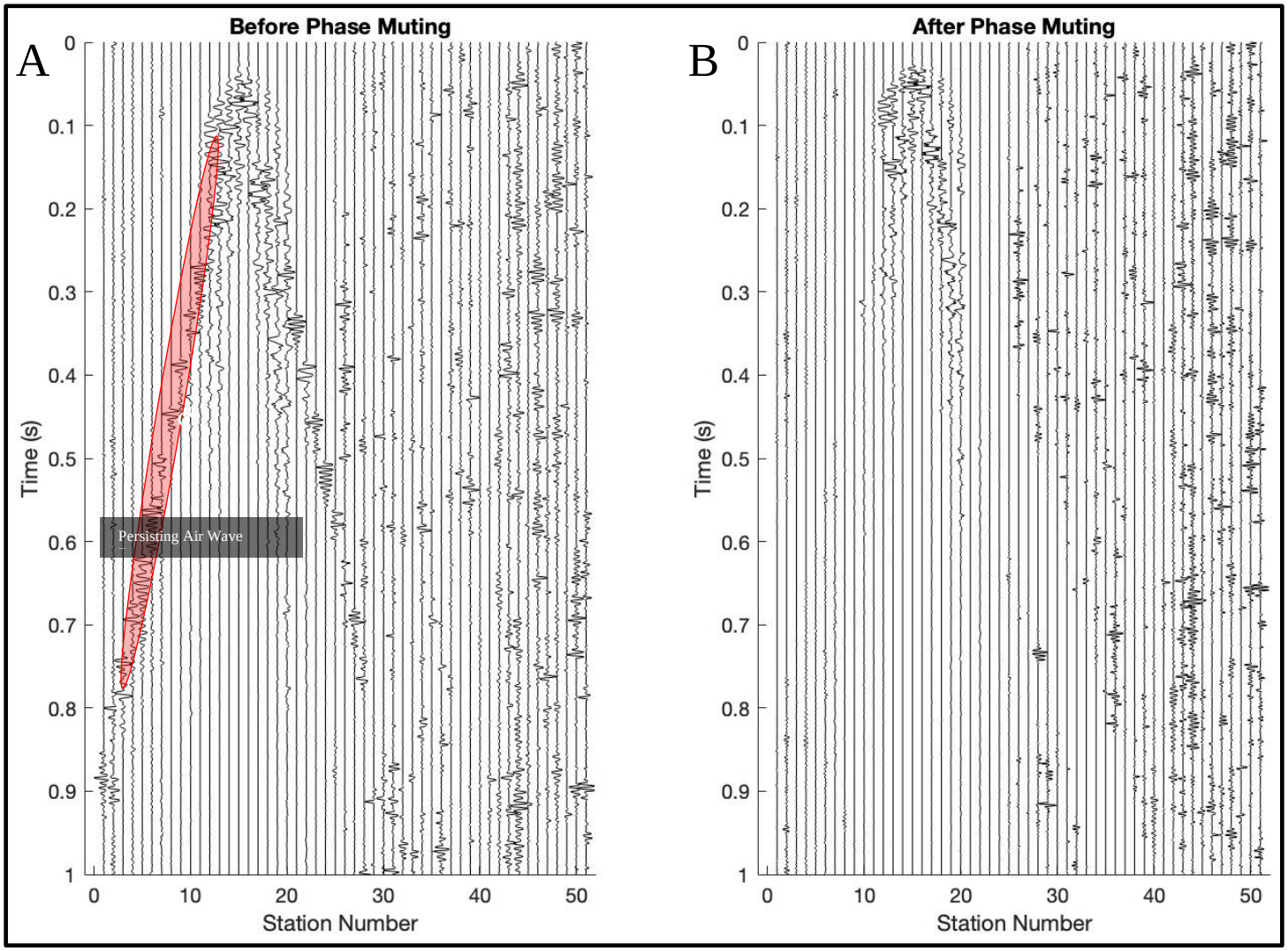

Figure 9: Before (A) and after (B) shot group 11 has been processed using phase muting. The persisting air wave energy is label in panel A, and has been removed in panel B.

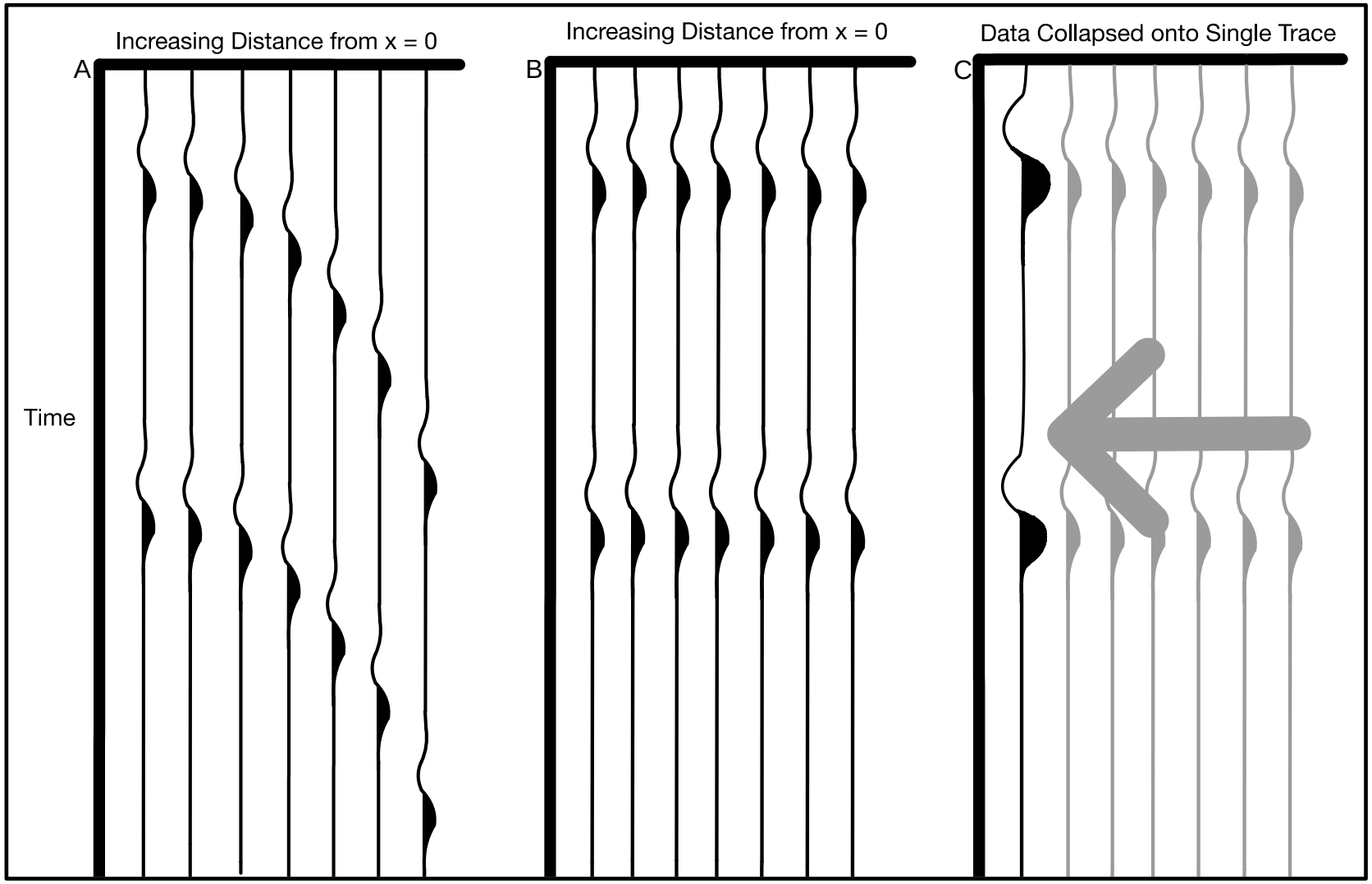

Figure 10: Simple depiction of taking the newly processed grouping of traced that share a common midpoint (A), what they look like after a normal moveout correction has been executed on them (B), and then how they are eventually collapsed/ stacked onto a single trace (C).

5 Analysis and Results

5.1 Seismic Line 1A

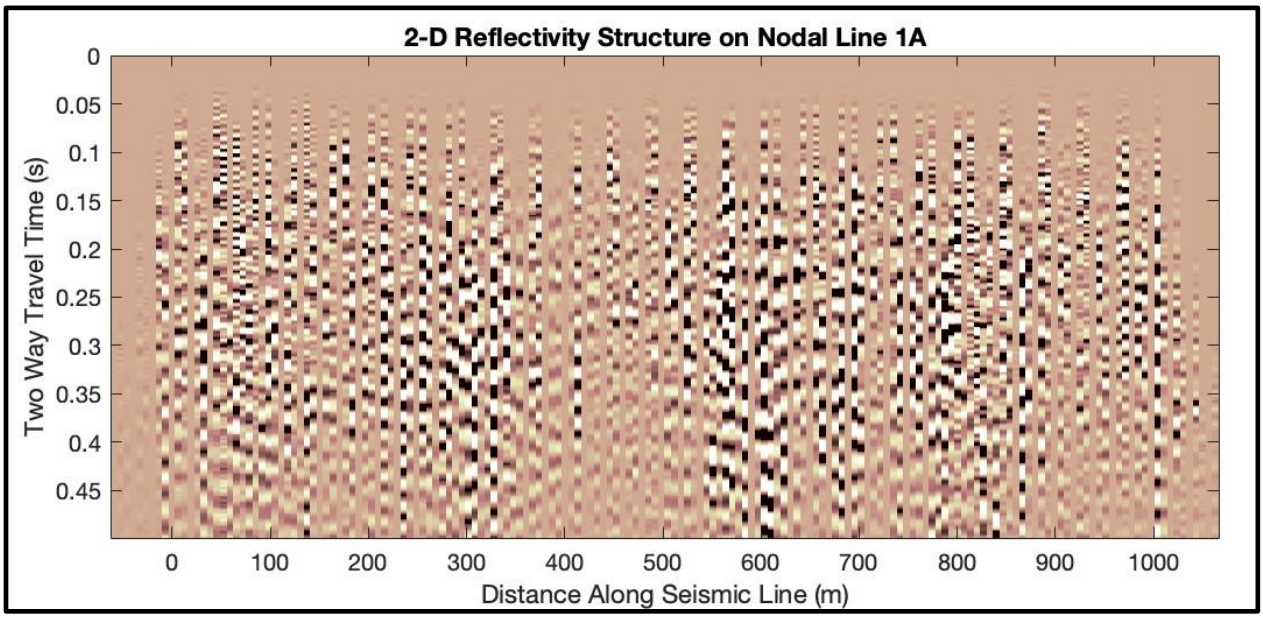

Figure 11: The 2-D Seismic structure underneath Seismic Line 1A.

Figure 11 shows the resulting 2-D cross section indicating the reflectivity structure of the subsurface under seismic line 1A. The reflectivity structure appears to be incoherent, and no direct geologic interpretation could be made from this result. Noticeably, there is a portion of low amplitude waves incoming at stations between 300 meters and 600 meters. To investigate this further, Figure 12A shows the envelope of the data, which essentially displays a 2-D map of the wave energy at each position in our cross section. It is evident by the figure that less energy is present in the area outlined by the white dashed line. The amplitude contrast between the high energy zone and the low energy zone can tell us about the overall wave attenuation the seismic waves experience during their time on the ray path. Note that the stripe of seemingly low energy at the top of the figure is intentionally put in to mute the over saturated direct waves.

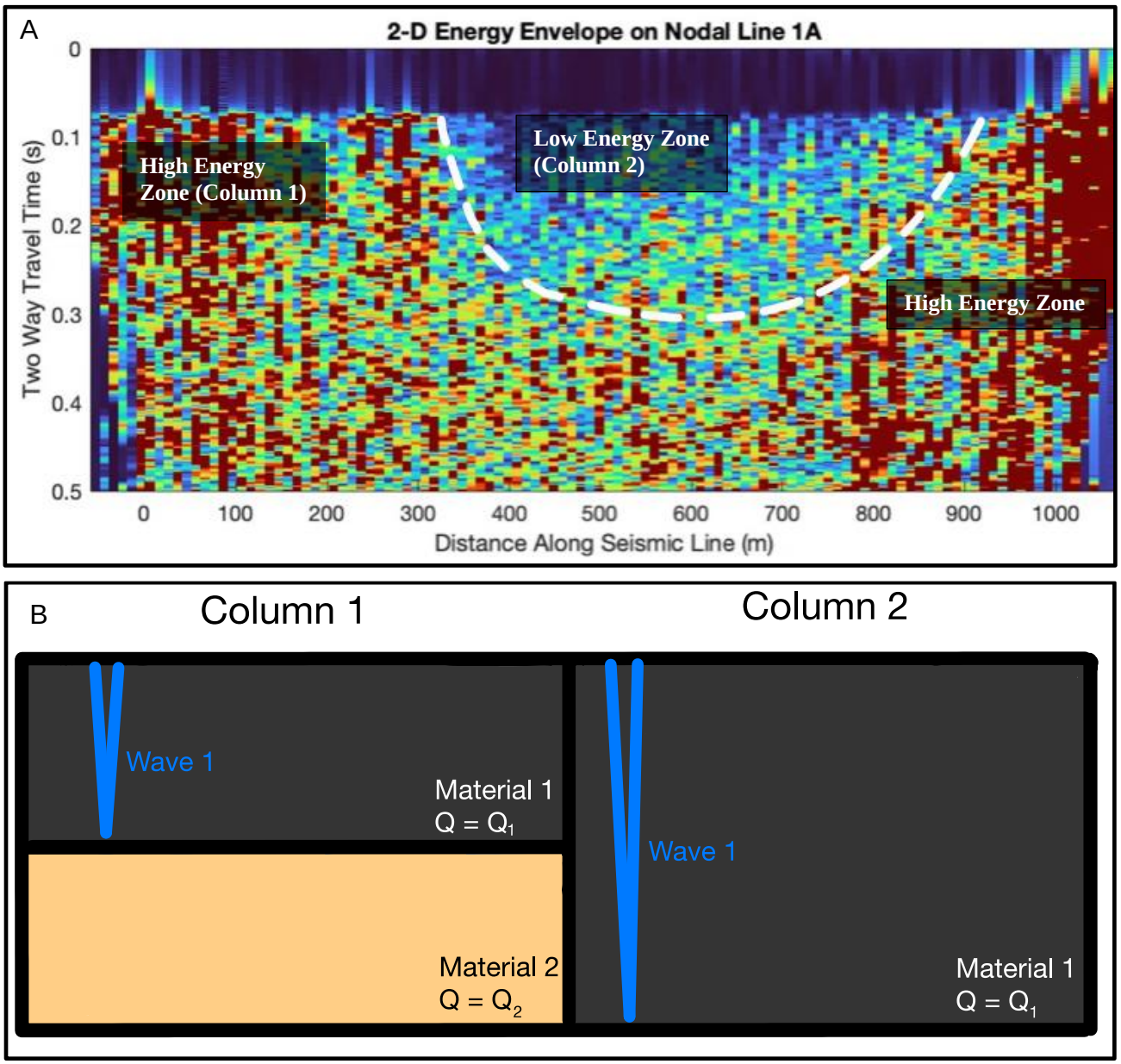

Figure 12: 2-D energy envelope of the data for seismic line 1A (A). Annotated are the different type of energy zone that represent the hypothetical two columns of material (B).

Let us imagine these zones represent the two columns in Figure 12B, with column one containing both material 1 and 2, and column two being entirely comprised of material 1. When seismic waves travel through any material, the amplitude of the wave at any given point can be calculated using the following formula:

$$A = A_0 e^{\frac{-\omega x}{2cQ}}$$

where A_0 is the initial amplitude of the wave, ω is the angular frequency of the wave, x is ray path distance, c is seismic wave velocity, and Q is the quality factor (Shearer, 2019). The quality factor is an observed value that measures how resistant a medium is to wave attenuation. Through these equations its evident that if a wave spends a larger portion of

its ray path, x, in a high attenuation layer, low Q, then the resulting amplitude would be smaller than if it spent less of its ray path inside that layer.

Given that our data have been organized such that each trace represents a ray path that has travelled directly down through the subsurface and travelled back, otherwise known as a zero-offset model, we can consider two waves, wave 1 and wave 2, that travel in this manner through each column (Figure 12B). If we consider each wave to only differ in ray path distance within material 1, then it would be expected to observe a portion of low amplitude waves being recorded in column two.

Figure 13 shows how rapidly wave amplitude would decrease as ray path in a layer with varying Q increases, relative to an original wave amplitude $A_0 = 1$. Given that the depth to the interface under seismic line 1A is approximately 40 meters, and the graben is predicted to have subsided an additional 40 meters, we can plot the two possible ray path distances through material 1. The intersections each Q line makes with these two vertical lines provide us with a ratio of amplitudes that should be observed for a given Q. Taking this data and plotting it onto Figure 14 shows how the amplitude ratio of two identical waves with different ray path lengths decrease as the quality factor increases. The formula for the curve is derived as follows:

$$\frac{A_1}{A_2} = \frac{A_0 e^{\frac{-\omega x}{2cQ}}}{A_0 e^{\frac{-\omega x}{2cQ}}}$$

$$\frac{A_1}{A_2} = e^{\frac{-\omega}{2cQ}(x_2 - x_1)}$$

$$\frac{A_1}{A_2} = e^{\frac{-\omega}{2cQ}\Delta x}$$

where x_2 and x_1 are the predicted ray path lengths, which for seismic line 1A are $x_2 = 160$ for column two and $x_1 = 80$ for column one. The angular frequency and wave velocity are fixed given that we are considering the same type of wave travelling through the same material. Q is allowed to vary to provide the x axis of the plot. Note that the ratio of amplitudes does not depend on the actual ray path distance, or depth of layer, but rather the difference between the two ray path distances. The quality factor (Q) of this material can be determined by working backwards through this equation. The average amplitudes, found by averaging all measurements recorded in each zone, in the high and low energy zones provides $A_1 = 0.00599 \pm 0.00009$ and $A_2 = 0.00127 \pm 0.00001$, respectively. The uncertainty in these measurements, ΔA_n, are found by:

$$\Delta A_n = \frac{\sigma}{\sqrt{N-1}}$$

where σ is the standard deviation of the measurments, and N is the number of measurements. This provides the average amplitude ratio of $f(A_1, A_2) = \frac{A_1}{A_2} = 4.71654 \pm 0.04006$, indicated by the red dashed line (Figure 14). The uncertainty in this value is found by the equation:

$$\Delta f(A_1, A_2) = \sqrt{\frac{\partial f}{\partial A_1}^2 \Delta A_1^2 + \frac{\partial f}{\partial A_2}^2 \Delta A_2^2}$$

This line intersects our curve at Q = 20.2.

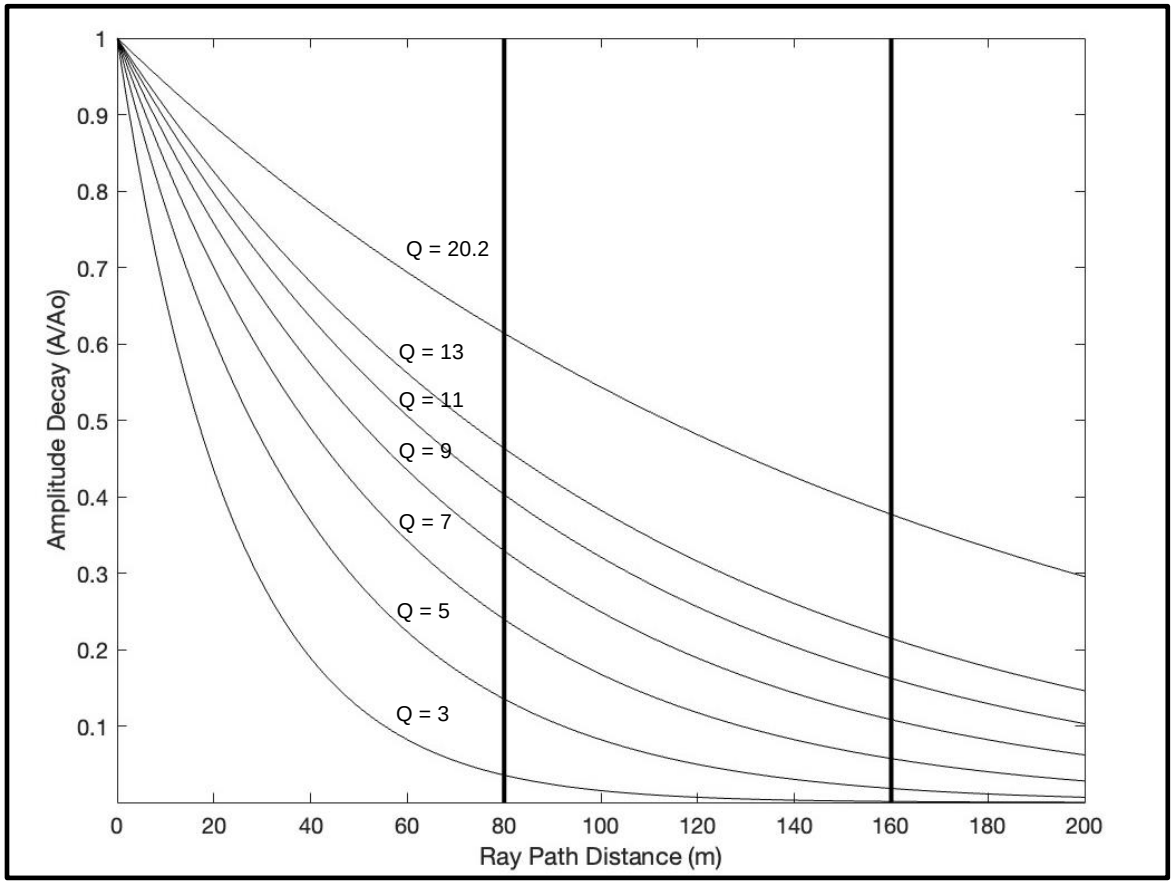

Figure 13: Plot indicating how rapid wave amplitude and energy decays as a function of increasing ray path distance. Plotted on the axes are the rate at which amplitudes decay depending on the labelled quality factor.

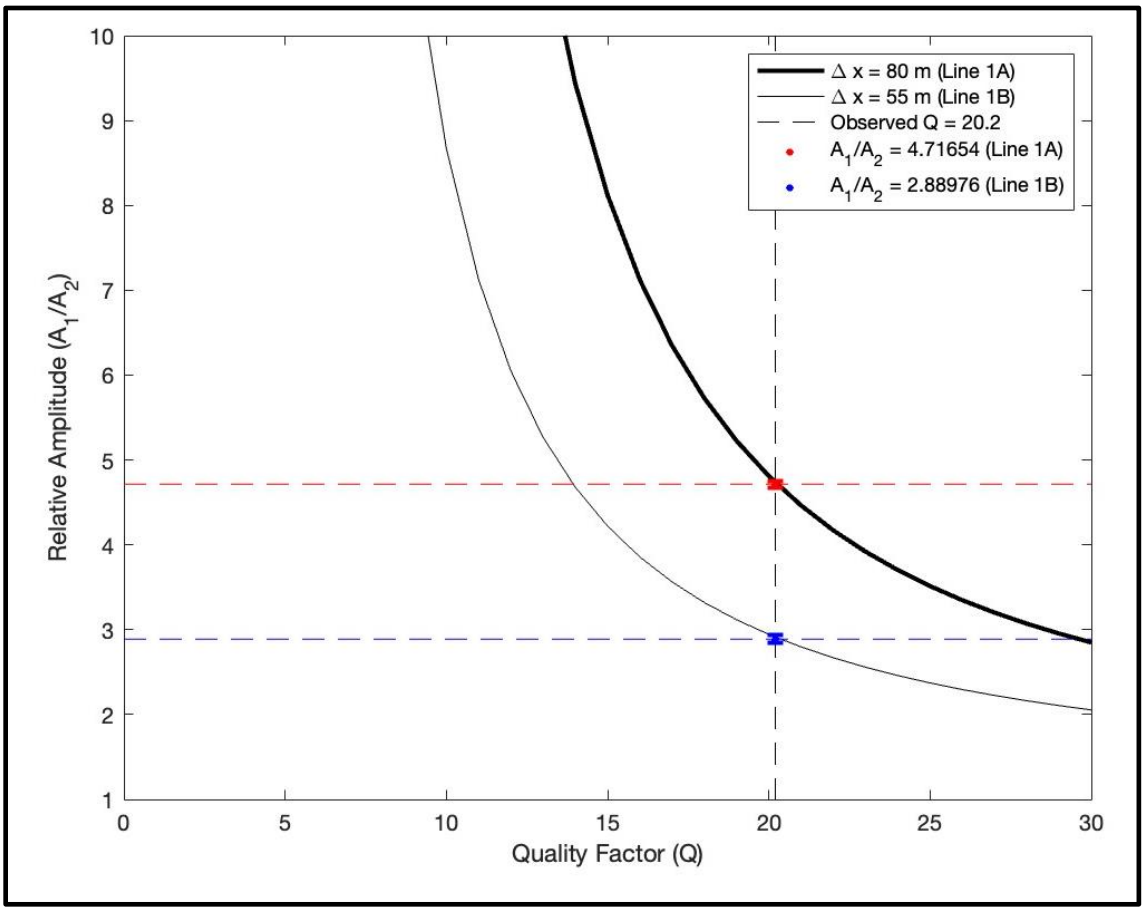

Figure 14: Graph indicating how the amplitude of one wave decays relative to another wave as a function of Q. Plotted are two solid black lines indicating varying difference in ray path within a highly attenuating material. Plotted in red and blue are the observed relative amplitudes between waves recorded at the high and low energy zones at seismic line 1A and 1B, respectively. Error bars are included in this graph.

5.2 Seismic Line 1B

Seismic line 1B produced a 2-D reflectivity structure similar to seismic line 1A in the sense that not much could be directly derived from the result (Figure 15). However, when plotting the envelope of the data to observe the map of wave energy, another low energy zone appears that was less evident in the reflectivity structure (Figure 16). Following a similar process for the prior line, it was found that the average amplitudes for the high and low energy zones are $A_1 = 0.00367 \pm 0.00007$ and $A_2 = 0.00127 \pm 0.00002$, respectively. This provides the average amplitude ratio to be $f(A_1, A_2) = \frac{A_1}{A_2} = 2.88976 \pm 0.04934$, and this is plotted with the blue dashed line in Figure 14. Taking the quality factor to be the same and adjusting Δx until the curve crossed the intersection of the blue dashed line and the black dashed line marking Q = 20.5 provides $\Delta x = 55$.

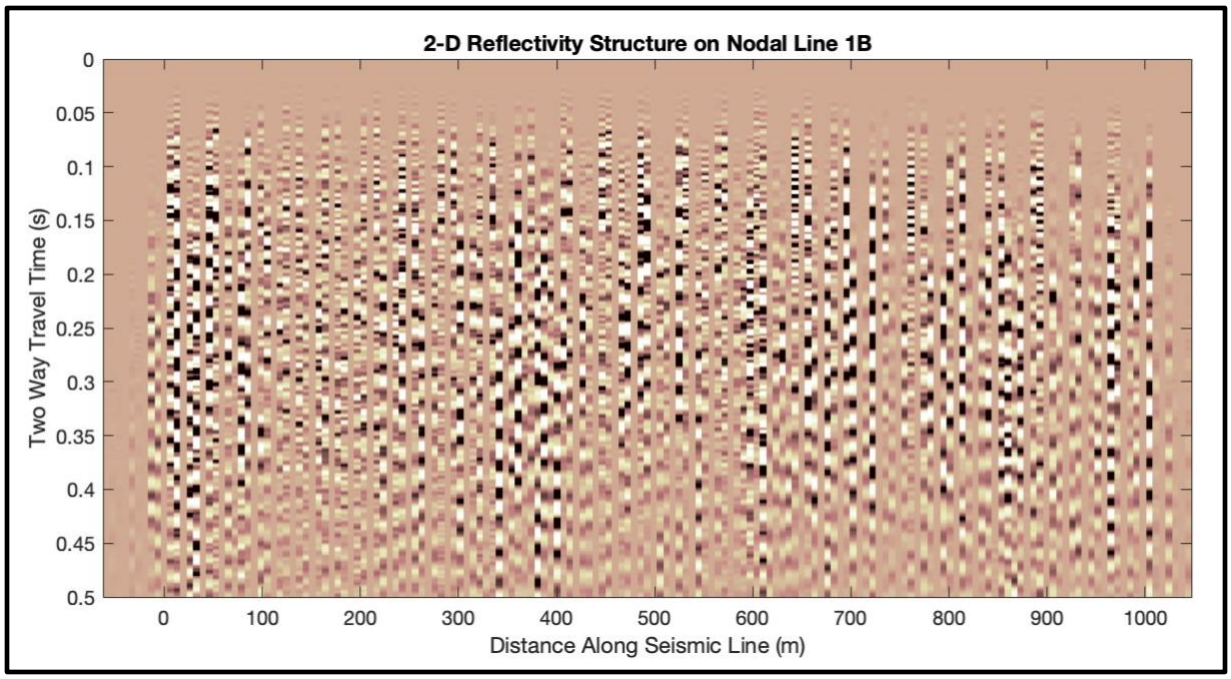

Figure 15: The 2-D Seismic structure underneath Seismic Line 1B.

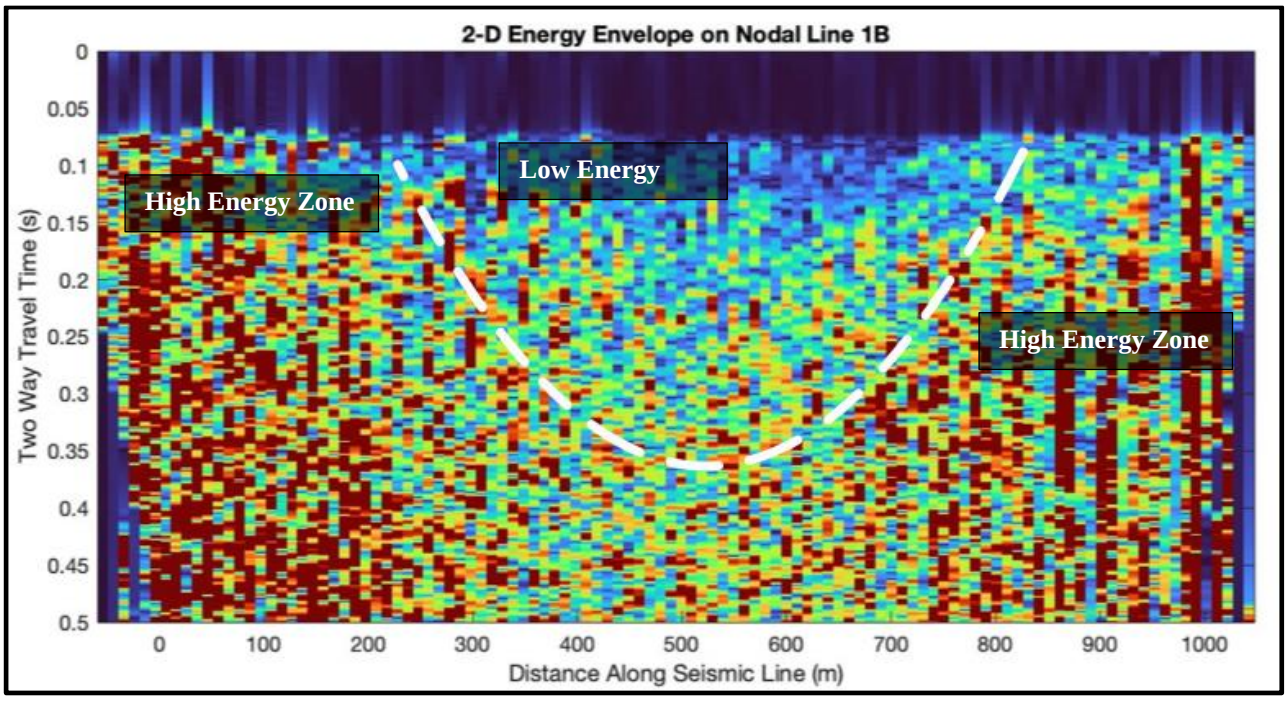

Figure 16: 2-D energy envelope of the data for seismic line 1B. Annotated are the different type of energy zones discussed through the present study.

6 Discussion

The original objective of the processing steps, to develop a 2-D map of the reflectivity structure below our two sites, resulted in incoherent reflectivity structures likely due to significant levels of attenuation and back scattering from the overlaying lava flows. Research has shown that the volcanic flows within the SFVF is subject to high seismic wave attenuation (Bell, 2021). Additionally, the source and receiver geometry were initially set up for a seismic refraction analysis, which benefits from a long seismic line and depends less on close receiver separation. A more beneficial receiver placement would have the receivers closer together and more localized near where the faults are predicted to be.

However, by studying the energy and average amplitudes of different locations along the line, the present study was able to identify evidence of H1 and the presence of the graben in close proximity to the seismic lines. Using this process, it was calculated that the quality factor of the top layer of material was approximately 20.2. This finding was consistent with previous studies on basaltic lava flows that revealed quality factors ranging from 10 to 60, depending on the type of basalt and level of hydration (Clarke et al., 2020; Di Martino et al., 2021; Maresh et al., 2006)

The 2-D Energy Envelope figures provide evidence that there is laterally inconsistent thickness of a highly attenuating material, the lava flows in the region, just beneath the surface at Seismic Lines 1A and 1B. For seismic line 1B, it was determined that in order to fit the curve to the intersection of the observed amplitude ratio and the measured quality factor, the difference in ray path distance, Δx, is approximately 55 meters. These findings are consistent with a SP Graben continuing underneath the subsurface and reaching the area beneath volcanic vent V5704. The difference between Δx for the calculations done on each line indicate that the graben and its associated faults are tapering off and reaching a terminus. The 3-D model in Figure 17 provides one possible visual interpretation of this structure in the region.

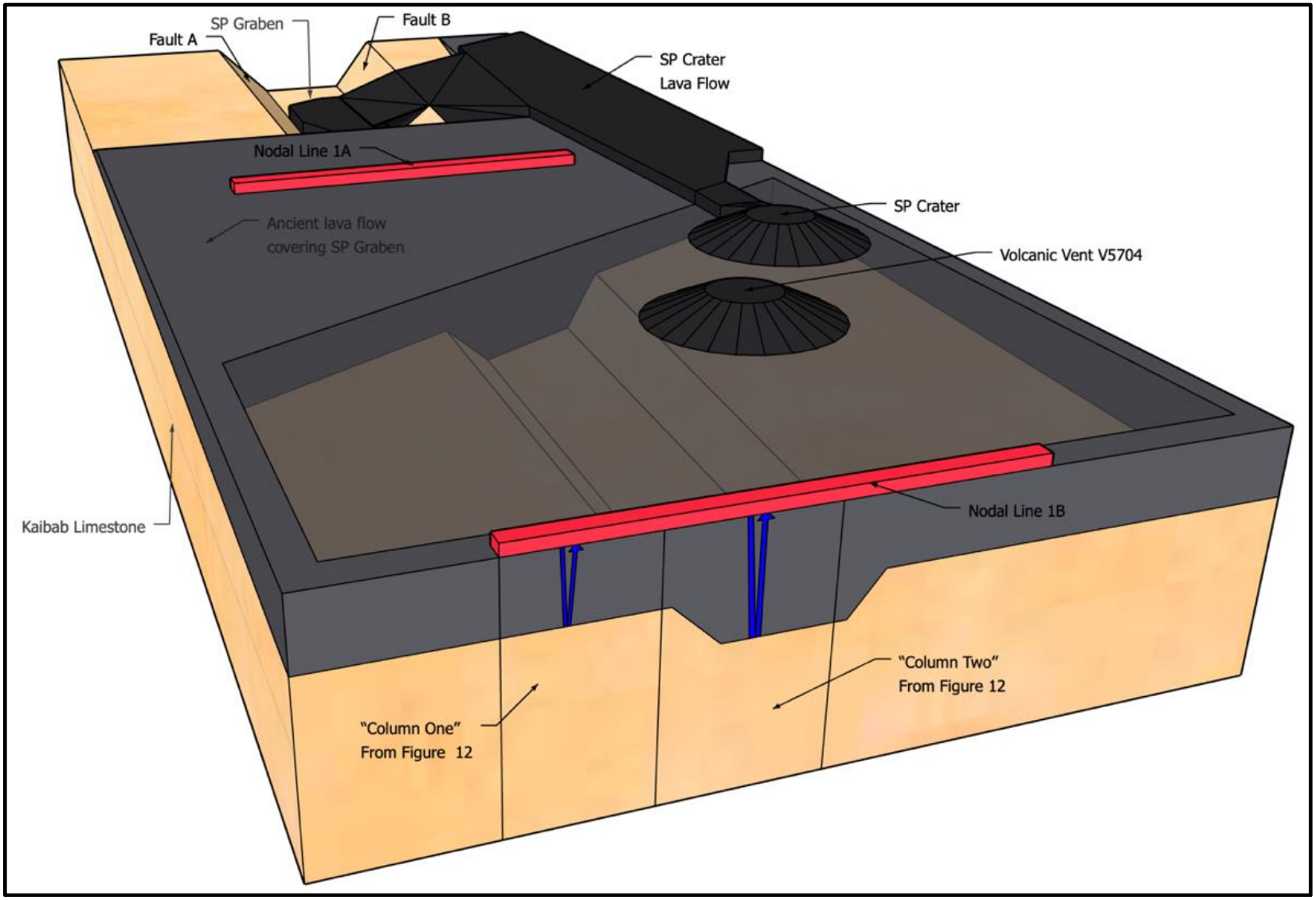

Figure 17: A 3-D rendering of what the geological structures could look like beneath the lava flows near SP Crater and Volcanic Vent V5704. Depicted are notable geological features and layers in the area. Note: Near the bottom of the image are labels for what is the physical manifestation of the hypothetical two column scenario used in Figure 12*

7 Conclusions

This analysis choose to explore the SFVF because of its unique geological features and scientific potential as a terrestrial analog site. This region possesses a fascinating geological history, which includes the uplift of the Colorado Plateau and the subduction of the Farallon Plate, resulting in a landscape covered in fractures, volcanoes, and lava flows (Mickus and Durrani, 1996; Van der Lee, Nolet, 1997). Given these distinctive features, the SFVF presents an ideal location for conducting research in conditions that may be observed when performing scientific investigations on the moon or Mars.

The primary objective of this investigation was to utilize a seismic data processing workflow to investigate the presence the SP Graben beneath SP Crater, which could be similar to scientific objectives that will be established for exploring the moon and Mars in the future. By demonstrating the capability to detect this graben, the study provides promise in using this process for future applications in space.

To achieve this objective, the present study employed a comprehensive seven-step process, which included resampling/cutting traces, common midpoint grouping, frequency and polarization filtering, normalizing, phase muting, and normal moveout correction. Using this approach, the present study was able to detect a thickening of the topmost geological layer, which is comprised of highly attenuating basaltic lava flows observed at the surface. However, this high attenuation also contributed to the incoherency of the intended results, the 2-D reflectivity structures.

Despite this challenge, through the wave attenuation analysis, it was shown that seismic waves on one area of the seismic lines were experiencing more attenuation than others, which can only be consistent with a sudden thickening of the lava flow layer along the direction of the seismic line, followed by a sudden thinning. This variation in lava flow thickness is believed to be a result of SP Graben being present at both seismic lines, providing evidence for H1. These results indicate that the processes in this study can inform future scientific investigations on the moon and Mars and can aid the scientific community in the future to better understand the geological processes that shape our solar system.

Acknowledgments

I would like to thank Dr. Nicholas Schmerr for working with me through this project. The hours spent writing on note pads and chalk boards were instrumental in the completion of this project. I would like to thank Dr. Vedran Lekic for helping me with this project and bringing the polarization filter/analysis to my field of view. This was by far my favorite analysis step to learn. I would like to thank Dr. Phillip Piccoli for always being available to discuss the project when I had a question or just to chat. Finally, I would like to thank the entire geology faculty for giving their time and interest in learning about my project and providing me feedback on how I can improve as a researcher.

References

Bell, J. E. (2021). Geophysical Exploration of Terrestrial and Lunar Volcanic Fields. [Doctoral Dissertation, University of Maryland – College Park] https://doi.org/10.13016/po0c-mhot

Billingsley, G. H., Priest, S. S., & Felger, T. J. (2007). Geologic Map of the Cameron 30’ x 60’ Quadrangle, Coconino County, Northern Arizona. United States Geological Survey. Map No. 2977.

Clarke, J., Adam, L., van Wijk, K., & Sarout, J. (2020). The influence of fluid type on elastic wave velocity and attenuation in volcanic rocks. Journal of Volcanology and Geothermal Research, 403. https://doi.org/10.1016/j.jvolgeores.2020.107004

Cooper, M. R., Kovach, R. L., & Watkins, J. S. (1974). Lunar near-surface structure. Reviews of Geophysics, 12(3), 291. https://doi.org/10.1029/RG012i003p00291

Di Martino, M., De Siena, L., Healy, D., & Vialle, S. (2021). Petro-mineralogical controls on coda attenuation in volcanic rock samples. Geophysical Journal International, 226, 1858-1872. https://doi.org/10.1093/gji/ggab198

Flowers, R. M. (2010). The enigmatic rise of the Colorado Plateau. Geology, 38(7), 671–672. https://doi.org/10.1130/focus072010.1

Gruener, J.E., Lofgren, G.E., Bluethmann, W.J., & Abercromby A.F. (2013). NASA Desert RATS 2010: Preliminary results for science operations conducted in the San Francisco Volcanic Field, Arizona. Acta Astronautica. 90(2), 406-415. https://doi.org/10.1016/j.actaastro.2011.12.006.

Le Corvec, N., Sporli, K. B., Rowland, J., & Lindsay, J. (2013). Spatial distribution

and alignments of volcanic centers: Clues to the formation of monogenetic volcanic fields. Earth-Science Reviews, 124, 96–114. https://doi.org/10.1016/j.earscirev.2013.05.005

Maresh, J., White, R. S., Hobbs, R. W., & Smallwood, J. R. (2006). Seismic attenuation of Atlantic margin basalts: Observations and modeling. Geophysics, 71, 211-221. https://doi.org/10.1190/1.2335875

Margrave, G. F. (2019). CREWES MATLAB Software Library [Computer software]. Retrieved from https://www.crewes.org/ResearchLinks/FreeSoftware/

Mickus, K. L., & Durrani, B. (1996). Gravity and magnetic study of the crustal structure of the San Francisco volcanic field, Arizona, USA. Tectonophysics, 267(1–4), 73–90. https://doi.org/10.1016/S0040-1951(96)00087-X

Montalbetti, J. F., & Kanasewich, E. R. (1970). Enhancement of Teleseismic Body Phases with a Polarization Filter. Geophysical Journal International, 21(2), 119-129.

National Aeronautics and Space Administration. (1969). Apollo 11 Mission Operations Report (No. M-932-69–11). Retrieved from https://www.hq.nasa.gov/alsj/a11/A11_MissionOpReport.pdf

National Aeronautics and Space Administration. (1970). Apollo 12 Mission Report (No. MSC-01855). Retrieved from https://www.hq.nasa.gov/alsj/a12/A12_MissionReport.pdf

National Aeronautics and Space Administration. (1976). Apollo 14 and 16 active seismic

experiments & Apollo 17 lunar seismic profiling. (No. N76-25140). Retrieved from https://ntrs.nasa.gov/api/citations/19760018052/downloads/19760018052.pdf

Priest, S. S., Duffield, W. A., Malis-Clark, K., Hendley II, J. W. & Stauffer, P. H. (2001). The San Francisco volcanic field, Arizona. U.S. Geological Survey Fact Sheet , 017-01, 2 p.

R.T. Clark Geophysical Equipment Co. (2014). PEG-40kg Brochure. Retrieved from https://rtclark.com/wp-content/uploads/2015/05/PEG-40kg-Brochure-2014.pdf

Rittenour, T. M., Riggs, N. R., & Kennedy, L. E. (2012). Application of Single-grain OSL to Date Quartz Xenocrysts within a Basalt Flow, San Francisco Volcanic Field, Northern Arizona, USA. Quaternary Geochronology, 10, 300-307

Romig, B., Kosmo, J., Ross, A., Bernard, C., Aitchison, L., Eppler, D., & Splawn, K. (2007). Desert Research and Technology Studies 2006 Report. SAE Transactions, 116, 170–193. http://www.jstor.org/stable/44719455

Shearer, P. M. (2019). Introduction to seismology. Cambridge university press.

Tanaka, K. L., Shoemaker, E. M., Ulrich, G. E., & Wolfe, E. W. (1986). Migration of volcanism in the San Francisco volcanic field, Arizona. Geological Society of America Bulletin, 97(2), 129. https://doi.org/10.1130/0016-7606(1986)97<129:MOVITS>2.0.CO;2

Tanaka, K. L., Skinner, J. A., Crumpler, L. S., & Dohm, J. M. (2009). Assessment of planetary geologic mapping techniques for Mars using terrestrial analogs: The SP Mountain area of the San Francisco Volcanic Field, Arizona. Planetary and Space Science, 57(5-6), 510-532. https://doi.org/10.1016/j.pss.2008.06.012.

Van der Lee, S., & Nolet, G. (1997). Seismic image of the subducted trailing fragments of the Farallon plate. Nature, 386, 266-269. https://doi.org/10.1038/386266a0

ZSystems Zland 1C and 3C Node User Manual. (2014). Fairfield Nodal.

Appendix

Below is the code utilized to process the data for this report. This code was developed by Professor Nicholas Schmerr for general reflection seismic processing and utilizes the MATLAB Crewes software. I made additions to the processing steps and edited the code to fit the needs of this report.

```
clear all; close all;


% Script to process SEG2 Data files


% This requires the MATLAB Crewes software to be installed on your machine
% https://www.crewes.org/ResearchLinks/FreeSoftware/
% Uses seg2load to read in SEG2 files, must be in your path


% Location of Matlab Radon Transform Codes:
% References: Schultz, R., Gu, Y. J., 2012. Flexible Matlab implementation
%           of the Radon Transform.  Computers and Geosciences [In
%           Preparation]%
%
%           An, Y., Gu, Y. J., Sacchi, M., 2007. Imaging mantle
%           discontinuities using least-squares Radon transform.
%           Journal of Geophysical Research 112, B10303.


%%%%%%%%%%%%%%%%%%%%%%%%%%%%  User Inputs
%%%%%%%%%%%%%%%%%%%%%%%%%%%%%%%%%%%%%%%


% Options for Preprocessing:
options=[];


% Data Location of SEG2 Files
dirpath='/Volumes/UNTITLED/ShotGathers/nodeline7_segy/';
%dirpath='/Volumes/UNTITLED/ShotGathers/nodelin11_segy/';


% This is file that contains a header with 12 lines delineating the
% experiment details, followed by 10 columns with the following format:
%  1       2       3       4     5    6     7      8         9
% LineN GeoPh_St GeoPh_End SrcLoc(m) Stack SrcLon SrcLat SrcElv(m) Filename
```

```
infofile = '/Volumes/UNTITLED/ShotGathers/nodeline7_segy/Meta7/sources_Site07.txt';%
%infofile = '/Volumes/UNTITLED/ShotGathers/nodeline11_segy/Meta11/sources_Site11.txt';

% This is file that contains a single header line and the location of the
% geophone stations in each seismic line
%   1            2           3           4         5     6
% StatLat      StatLon     StatElv(m)    StatLoc(m)  StatN  LineN
recsfile = '/Volumes/UNTITLED/ShotGathers/nodeline7_segy/Meta7/stations_Site07.txt';
%recsfile = '/Volumes/UNTITLED/ShotGathers/nodeline11_segy/Meta11/stations_Site11.txt';

% 1) Data Resampling (Use this if your records are quite long or high
% sampling rate... could add an option to also cut length?
options.dataresample = 1; % Switch to turn on or off (1=on, 0=off)
options.Fs_new = 1000; % New Sampling rate desired (Hz)


% 2) Cutting the data to a new time window (currently best to use 0 for the
% first time window cut)
options.datacut = 1;
options.datacutwin = [0 2];
info = readtable(infofile,'HeaderLines',13,'ReadVariableNames',0); % Make sure this matches in your file
recs = readtable(recsfile,'HeaderLines',1,'ReadVariableNames',0);


%%%%%%%%%%%%%%%%%%%  End of User Inputs
%%%%%%%%%%%%%%%%%%%%%%%%%%%%%%%%%%%%

%% Read in the Experiment Metadata and Data
info = readtable(infofile,'HeaderLines',13,'ReadVariableNames',0); % Make sure this matches in your file
recs = readtable(recsfile,'HeaderLines',1,'ReadVariableNames',0);

data=[];

% Initialize the Array
CMPdata=[];
CMPdata.X       = [];
CMPdata.D       = [];
```

```
CMPdata.M        = [];
CMPdata.S        = [];
CMPdata.statlats = [];
CMPdata.statlons = [];
CMPdata.statelev = [];
CMPdata.srclats  = [];
CMPdata.srclons  = [];
CMPdata.srcelev  = [];
CMPdata.midplats = [];
CMPdata.midplons = [];
CMPdata.midpelev = [];
CMPdata.traces   = [];
CMPdata.Fs       = [];
CMPdata.T        = [];
CMPdata.src_elev = [];
CMPdata.stat_elev= [];

tic; % Time it
for i=1:size(info,1)

    % Load all the Data into a Structure
    data{i}.seg2file = info.Var9{i}; % SEG2 Filename
    data{i}.line     = info.Var1{i}; % Line #
    data{i}.stack    = info.Var5(i); % # Stacked Shots
    data{i}.srclon   = info.Var6(i); % Source Longitude
    data{i}.srclat   = info.Var7(i); % Source Latitude
    data{i}.srcelev  = info.Var8(i); % Source Elevation
    data{i}.srcloc   = info.Var4(i); % Source Location (m)
    data{i}.x1       = info.Var2(i); % Geophone 1 position (m)
    data{i}.x2       = info.Var3(i); % Geophone n position (m)

    % Then assign all the details into the structures below:
    %%%%%%%%

     % Read in SEG2 file to trace and header info
    [data{i}.trace,data{i}.header]=seg2load([dirpath,data{i}.seg2file]);
```

```
%%%%%%%%%%%%%%%%%%%%%%%%%%%%%%%%%%%%%%%%%%%%%%%%%%%%%%%%%%%%
%%%%%%%%%%%%%
  % Downsample the data to a new resampling rate
  if (options.dataresample == 1)
    % Get the current record information
    sampint = max(data{i}.header.tr.sampling);
    delay   = max(data{i}.header.tr.delay);
    npts    = size(data{i}.trace,1);
    Fs      = 1/sampint; % Hz
    Fnyq    = 0.5*1/sampint; % Hz
    Tstart = 0-delay;
    Tend   = Tstart+npts*sampint;
    T      = linspace(Tstart,Tend,npts);

    Tq = min(T):1/options.Fs_new:max(T);
    traceq = interp1(T,data{i}.trace,Tq);

    % Replace the amplitude matrix
    data{i}.trace = traceq;

    % Sampling interval
    data{i}.sampint=1/options.Fs_new;

    % Start delay
    data{i}.delay=delay;

    % Size of the trace
    data{i}.npts=size(traceq,1);

    % Sampling Frequency
    data{i}.Fs   = 1/data{i}.sampint; % Hz
    data{i}.Fnyq = 0.5*1/data{i}.sampint; % Hz

    % Time vector
    data{i}.Tstart = 0-data{i}.delay;
```

```
        data{i}.Tend   = data{i}.Tstart+data{i}.npts*data{i}.sampint;
        data{i}.T      = linspace(data{i}.Tstart,data{i}.Tend,data{i}.npts);
        clear sampint delay npts Fs Fnyq Tstart Tend T Tq traceq;

    else % Just do things normally

        % Sampling interval
        data{i}.sampint=max(data{i}.header.tr.sampling);

        % Start delay
        data{i}.delay=max(data{i}.header.tr.delay);

        % Size of the trace
        data{i}.npts=size(data{i}.trace,1);

        % Sampling Frequency
        data{i}.Fs   = 1/data{i}.sampint; % Hz
        data{i}.Fnyq = 0.5*1/data{i}.sampint; % Hz

        % Time vector
        data{i}.Tstart = 0-data{i}.delay;
        data{i}.Tend   = data{i}.Tstart+data{i}.npts*data{i}.sampint;
        data{i}.T      = linspace(data{i}.Tstart,data{i}.Tend,data{i}.npts);


    end
    % End of Trace Resampling

%%%%%%%%%%%%%%%%%%%%%%%%%%%%%%%%%%%%%%%%%%%%%%%%%%%%%%%%%%%%%%%%%%%%%%%%%%%%%%%%%%%%%%%%%%%%%%%%%%%%%%%%%%%%%%%%%%%%%%%%%%%%%%%%%%%%%%%%%%%%%%%%%%%%%%%%%%%%%%%%%%%%%%%%%%%%%%%%%%%%%%%%%%%%%%%%
%%%%%%%%%%%%%%%%%%%%%%%%


%%%%%%%%%%%%%%%%%%%%%%%%%%%%%%%%%%%%%%%%%%%%%%%%%%%%%%%%%%%%%%%%%%%%%%%%%%%%%%%%%%%%%%%%%%%%%%%%%%%%%%%%%%%%%%%%%%%%%%%%%%%%%%%%%%%%%%%%%%%%%%%%%%%%%%%%%%%%%%%%%%%%%%%%%%%%%%%%%%%%%%%%%%%%%%%%
%%%%%%%%%%%%%%%%%%%%%%%%
    % Cut the data to a length
    if (options.datacut == 1)
        % Get the current record information
```

```
    sampint = max(data{i}.header.tr.sampling);
    delay   = max(data{i}.header.tr.delay);
    npts    = size(data{i}.trace,1);

    Fs      = 1/sampint; % Hz
    Fnyq    = 0.5*1/sampint; % Hz

    npts_win1 = floor(abs(options.datacutwin(1)-delay)/sampint)+1;
    npts_win2 = floor((options.datacutwin(2)-options.datacutwin(1))/sampint);

        if(npts_win2 > npts)
          npts_win2 = npts;
          DISP('Cut window exceeds length of seismogram, using NPTS from orginal file')
        end

    % Trim the file to the time window
    traceq = data{i}.trace(npts_win1:npts_win2,:);

    % Replace the amplitude matrix with the cut values
    data{i}.trace = traceq;

    % Replace with the new length of the trace
    data{i}.npts=size(traceq,1);

    % Replace the Time vector
    data{i}.Tstart = options.datacutwin(1);
    data{i}.Tend   = data{i}.Tstart+data{i}.npts*data{i}.sampint;
    data{i}.T      = linspace(data{i}.Tstart,data{i}.Tend,data{i}.npts);
    clear sampint delay npts Fs Fnyq Tstart Tend T Tq traceq;
  end
  % End of Trace Cutting

%%%%%%%%%%%%%%%%%%%%%%%%%%%%%%%%%%%%%%%%%%%%%%%%%%%%%%%%%%%%%%%%
%%%%%%%%%%%%%%

  % To normalize all the traces
  data{i}.maxval=max(max(data{i}.trace(:)));
```

```
    data{i}.minval=min(min(data{i}.trace(:)));

    % Station positions
    data{i}.nrecs  = data{i}.header.rec.traces_rec;

    % Get the matching geophone information from the recs file:
    vals=strmatch(data{i}.line,recs.Var6,'exact');

    data{i}.recs = recs(vals,:);
    clear vals
    data{i}.X      = data{i}.recs.Var4; % Assign station positions from station file
    data{i}.D      = data{i}.X-data{i}.srcloc; % Assign distances from station file
    data{i}.M      = data{i}.srcloc+0.5*(data{i}.X-data{i}.srcloc); % Find the location of the midpoint between source and
station

    % Location of the stations in lat and lon
    data{i}.statlats   = data{i}.recs.Var1;
    data{i}.statlons   = data{i}.recs.Var2;
    data{i}.statelev   = data{i}.recs.Var3;

    % Compute the location of the midpoints
    data{i}.midplats   = data{i}.srclat + 0.5*(data{i}.statlats-data{i}.srclat);
    data{i}.midplons   = data{i}.srclon + 0.5*(data{i}.statlons-data{i}.srclon);
    data{i}.midpelev   = data{i}.srcelev + 0.5*(data{i}.statelev-data{i}.srcelev);

    % Consolidate the Data into One Huge Datatable
    CMPdata.X        = [CMPdata.X; data{i}.X];
    CMPdata.D        = [CMPdata.D; data{i}.D];
    CMPdata.M        = [CMPdata.M; data{i}.M];
    CMPdata.S        = [CMPdata.S; zeros(size(data{i}.X))+data{i}.srcloc];
    CMPdata.statlats = [CMPdata.statlats; data{i}.statlats];
    CMPdata.statlons = [CMPdata.statlons; data{i}.statlons];
    CMPdata.statelev = [CMPdata.statelev; data{i}.statelev];
    CMPdata.srclats  = [CMPdata.srclats; zeros(size(data{i}.statlats))+data{i}.srclat];
    CMPdata.srclons  = [CMPdata.srclons; zeros(size(data{i}.statlons))+data{i}.srclon];
    CMPdata.srcelev  = [CMPdata.srcelev; zeros(size(data{i}.statelev))+data{i}.srcelev];
    CMPdata.midplats = [CMPdata.midplats; data{i}.midplats];
```

```
    CMPdata.midplons = [CMPdata.midplons; data{i}.midplons];
    CMPdata.midpelev = [CMPdata.midpelev; data{i}.midpelev];
    CMPdata.src_elev = [CMPdata.src_elev; data{i}.src_elev];
    CMPdata.stat_elev= [CMPdata.stat_elev; data{i}.stat_elev];

    % Grab some data information
    CMPdata.traces   = [CMPdata.traces; data{i}.trace'];
    CMPdata.Fs       = [CMPdata.Fs; zeros(size(data{i}.X))+data{i}.Fs];
    CMPdata.T        = [CMPdata.T;  zeros(size(data{i}.trace'))+data{i}.T];



end
toc
%--------------------------------------------------------------------------


%% Compute statics correction and Apply to the data

% Topography along the line
CMPdata.tshift = [];
CMPdata.shifted = [];

% Find the datum to correct to, this should be tied to the lowest elevation
% observed in the dataset (Hence why I am doing it here so that the datum
% doesn't change if the shot is lower (or higher) than the stations.
datum = min([CMPdata.src_elev; CMPdata.stat_elev]);

for i = 1:length(data)
    data{i}.tshift    = 1*(data{i}.src_elev+data{i}.stat_elev - 2*datum)./options.staticvel;
    CMPdata.tshift = [CMPdata.tshift; data{i}.tshift]; % Keep a vector with the time shifts
    pts = ceil(data{i}.tshift./data{i}.sampint);

    for j=1:length(pts)

      shifted = data{i}.trace(:,j)*0;
      ept = length(data{i}.trace(1+(pts-min(pts)):end,j));
```

```
      shifted(1:ept) = data{i}.trace(1+(pts-min(pts)):end,j);
      data{i}.shifted(:,j)=shifted;

   end
   CMPdata.shifted = [CMPdata.shifted; data{i}.shifted'];
end

%--------------------------------------------------------------------------


%% Assemble Common Midpoint Gathers

%[C,ia,ic]=unique(CMPdata.M); % This just finds the midpoints that have unique locations, it might be desirable to bin the data together?
% Creating coarser bin spacing for our CMPs of bin width DD/2 with lower
% and upper limit ll and ul respectively
ll = floor(min(CMPdata.M)); %
DD = 20;
ul = floor(max(CMPdata.M));
C = ll : DD/2 : ul;
ic = [];

for i=1:length(CMPdata.M)
   ic(i) = find(CMPdata.M(i) >= C & CMPdata.M(i) <= C+DD/2);
end

%ia => original categories
%ic => category C assigned to each value

CMPs=[]; f=[];

for i=1:length(C)

   vals = (ic == i); % Find the midpoints that match this CMP

   fold = length(find(vals > 0)); % Find the number of records in this CMP
```

```
    CMPs{i}.fold     = fold;
    CMPs{i}.X        = CMPdata.X(vals);
    CMPs{i}.D        = CMPdata.D(vals);
    CMPs{i}.M        = CMPdata.M(vals);
    CMPs{i}.S        = CMPdata.S(vals);
    CMPs{i}.statlats = CMPdata.statlats(vals);
    CMPs{i}.statlons = CMPdata.statlons(vals);
    CMPs{i}.statelev = CMPdata.statelev(vals);
    CMPs{i}.srclats  = CMPdata.srclats(vals);
    CMPs{i}.srclons  = CMPdata.srclons(vals);
    CMPs{i}.srcelev  = CMPdata.srcelev(vals);
    CMPs{i}.midplats = CMPdata.midplats(vals);
    CMPs{i}.midplons = CMPdata.midplons(vals);
    CMPs{i}.midpelev = CMPdata.midpelev(vals);
    CMPs{i}.traces   = CMPdata.traces(vals,:);
    CMPs{i}.Fs       = CMPdata.Fs(vals);
    CMPs{i}.T        = CMPdata.T(vals,:);
    CMPs{i}.O        = (CMPdata.X(vals)-CMPdata.S(vals)); % Reciever-Source Offset
    f = [f;fold]; % Keep track of the fold in the CMP stacks

end

%%
% Plots Up the Data Fold
figure;

subplot(2,1,1)
plot(C,f,'.');
xlabel('Midpoint Location (m)'); ylabel('N-Fold in CMP');

subplot(2,1,2)
plot(1:length(CMPs),f,'.');
xlabel('CMP #'); ylabel('N-Fold in CMP');

%--------------------------------------------------------------------------
%% Processing Steps
tic
```

```
%frequency and polarization filter
polar = 1;
smp = 1/options.Fs_new;
Nyq = (0.5)/smp;
flo = 75;
fhi = 200;
nord = 2;
dt        = 0.25/fhi;          % Set the desired sampling interval (4 samples at Fhi)
window_dur = 0.01;


% Normalize each record to 1
normalize = 1;

% Phase Muting
phasemute = 1; % 0=off/1=on For muting specific arrivals in the data
%cvel      = [250:20:600,950:25:1050];     % Velocities of waves to mute (m/s)
           %[LowerLim:Interval:UpperLim, next setio same format]
cvel = [250:20:400];
tw        = [0.05 0.15]; % Taper width in seconds [start stop]
tp        = 0.25;          % Taper percent

% Plotting Option Limits
climit=[-0.015 0.015];  % amplitude scaling
ylimit=[0 1]; % Time limit (for zooming)

% NMO Velocity (m/s)/Layering
v1 = 800;
v2 = 3000;

t1 = 0.08; %line7
%t1 = 0.175; %line11


% Plotting Figures
```

```
figplot = 0; % 0=off/1=on for plotting summary figures

%%%%%%%%%%%%%%%%%%%%%%%%%%%%%%%%%%%%%%%%%%%%%%%%%%%%%%%%%%
%%%%%%%%%%%%%%%%%
% Processing multiple shots
stack=[];
midpts=[];


load('/Users/austinhoyle/Desktop/green/SciColor/davos/davos.mat');

 %%%%%%%%%%%%%%%%%%%%%%%%%


 %%%%%%%%%%%%%%%%%%%%%%%%%
for cmp =  1:size(CMPs,2)

    shot=1; % Reference information
    %-----------------------------------------------------------------------
    % Raw Data
%    A    = data{shot}.trace;   % Amplitudes
%    X    = data{shot}.X;       % Station positions (m)
%    T    = data{shot}.T;       % Time (s)
%    S    = data{shot}.srcloc;  % Source location (m)
%    D    = data{shot}.D;       % Distances from source (m)

    % For processing a CMP gather:
    comp=(3:3:size(CMPs{cmp}.traces,1));
    A    = CMPs{cmp}.traces(comp,:)';   % Amplitudes - TRACES
    X    = CMPs{cmp}.X(comp);           % Station positions (m)
    T    = CMPs{cmp}.T(1,:);            % Time (s)
    S    = CMPs{cmp}.S(comp);           % Source location (m)
    D    = CMPs{cmp}.D(comp);           % Distances from source (m)
    M    = CMPs{cmp}.M(comp);           % Midpoint Location (m)
    O    = CMPs{cmp}.O(comp);           % Distance of station from Midpoint (m)

    midpts(cmp)=median(CMPs{cmp}.M);
```

```
% For RAW Data
if (figplot == 1)
    figure('Position',[0 0 720 720]);
    colormap(davos);
    pcolor(O,T,A./max(A));
    shading flat;

    % Label the Plot
    title(['RAW ',data{shot}.seg2file,' | ',data{shot}.line,' | ','shotloc (m): ',num2str(data{shot}.srcloc)])
    xlabel('Offset (m)'); ylabel('Time (s)');
    set(gca, 'YDir', 'reverse' ); set(gca,'FontSize',20);
    caxis(climit); ylim(ylimit);
    c=colorbar; c.Label.String = 'Amplitude [DU]';
    c.Location = 'eastoutside';
end

% Get the raw data "filt" is now filtered trace
filt=A;

%--------------------------------------------------------------------------

if polar == 1
    i = cmp;

    Zcomp=(3:3:size(CMPs{i}.traces,1));     % just making vectors that have "n"
    Ncomp=(3-2:3:size(CMPs{i}.traces,1)-2); % in each cell dependant on component
    Ecomp=(3-1:3:size(CMPs{i}.traces,1)-1);

    Zfilt = CMPs{i}.traces(Zcomp,:)'; %pulling out each trace and sorting based on comp
    Nfilt = CMPs{i}.traces(Ncomp,:)';
    Efilt = CMPs{i}.traces(Ecomp,:)';

    Zfilt =tukeywin(length(Zfilt),0.01).*(Zfilt); %filtering all three comps pt 1
    Nfilt =tukeywin(length(Nfilt),0.01).*(Nfilt);
    Efilt =tukeywin(length(Efilt),0.01).*(Efilt);
```

```
    [tmpZ,tmpP,tmpK] = butter(nord,[flo/Nyq fhi/Nyq],'bandpass');
    [SOS,G] = zp2sos(tmpZ,tmpP,tmpK); %filtering all three comps pt 2

    Nfilt = filtfilt(SOS,G,Nfilt); %filtering all three comps pt 3
    Efilt = filtfilt(SOS,G,Efilt);
    Zfilt = filtfilt(SOS,G,Zfilt);

    Zfreqfilt{i} = Zfilt; %placing filtered trace group into a new structure
    Nfreqfilt{i} = Nfilt; % that intervals as i increases
    Efreqfilt{i} = Efilt;

    window_pts = ceil(window_dur/dt);
    % %%%%%%%%%%%% Polarization filter - takes all three comps
    % and condenses down to a single component that is polarized
    % filtered
    for j=1:size(Zfreqfilt{i},2)
        Zcut = Zfreqfilt{i}(:,j); %Z
        Ncut = Nfreqfilt{i}(:,j); %T
        Ecut = Efreqfilt{i}(:,j); %R
        [Wvfrm_fil,RL_sm,D_sm,PA]=pzfilter([Ecut Ncut Zcut],window_pts);
        filt(:,j) = Wvfrm_fil(:,3); %setting output traces equal to filt for
                                %the rest of the code to process
    end
end
%-------------------------------------------------------------------------

%-------------------------------------------------------------------------
% Normalize to 1
if (normalize == 1)

    filt=filt./max(filt);

    % Correct the amplitudes

    % Plot the Result
    if (figplot == 1)
        figure('Position',[0 0 720 720]);
```

```
        colormap(davos);

        % Plot the Seismograms
        pcolor(O,T,filt); hold on;

        % Plot the location of the velocities used
        for i=1:length(cvel)
            plot(D,abs(D)/cvel(i),'.r');
        end

        % Label the Plots
        title(['Normalized ',data{shot}.seg2file,' | ',data{shot}.line,' | ','shotloc (m): ',num2str(data{shot}.srcloc)])
        xlabel('Offset (m)'); ylabel('Time (s)');
        set(gca, 'YDir', 'reverse' ); set(gca,'FontSize',20);
        caxis(climit); ylim(ylimit);
        c=colorbar; c.Label.String = 'Amplitude [DU]'; c.Location = 'eastoutside';
    end

end
%--------------------------------------------------------------------------

%--------------------------------------------------------------------------
% Phase muting
if (phasemute == 1)

    % Mute each velocity in cvel
    for j = 1:length(cvel)
        for i = 1:length(X)

            % Find the time window where the taper window exists
            Tm=((data{shot}.Tstart-tw(1)):data{shot}.sampint:(data{shot}.Tend+tw(2))); % Pad out the time vector for
cases where the taper exceeds the size of the orignal Time vector
            vals = find(Tm<=(abs(D(i))./cvel(j)+tw(2)) & Tm>=(abs(D(i))./cvel(j)-tw(1)));

            % Construct the taper
            Am=Tm*0+1; % Create a mute vector
            Am(vals)=(1-tukeywin(length(Am(vals)),tp)); % Taper the muted phase
```

```
            % Pick out the time window that exists in the data
            mute=Am(Tm >= data{shot}.Tstart & Tm < data{shot}.Tend);
            filt(:,i)=filt(:,i).*mute(1:length(T))';
        end
    end

    % Plot the Result
    if (figplot == 1)
        figure('Position',[0 0 720 720]);
        colormap(davos);

        % Plot the Seismograms
        pcolor(O,T,filt./max(filt)); hold on; shading flat;

        % Plot the location of the velocities used
        for i=1:length(cvel)
            plot(D,abs(D)/cvel(i),'.r');
        end

        % Label the Plots
        title(['PHASE MUTED ',data{shot}.seg2file,' | ',data{shot}.line,' | ','shotloc (m): ',num2str(data{shot}.srcloc)])
        xlabel('Offset (m)'); ylabel('Time (s)');
        set(gca, 'YDir', 'reverse' ); set(gca,'FontSize',20);
        caxis(climit); ylim(ylimit);
        c=colorbar; c.Label.String = 'Amplitude [DU]';
        c.Location = 'eastoutside';
    end

end
%--------------------------------------------------------------------------

%--------------------------------------------------------------------------
% Normal Moveout Correction

    v=T*0; % NMO velocity to use
```

```
% Layered Case (e.g., from a Velocity Analysis)

v(T<=t1)=v1; %Estimating interface @ 40 meters depth -AH
v(T>t1)=v2;
% Constant Velocity Case
%v=v*0+250;




% Amps/Time/Src-Rec offset/Velocity/RemoveNMORflag/ %to_use / %taper /cosine
P=(X-S);

sout=nmor(filt,T,P,v',1,[30 10.0 1]);

CMPs{cmp}.stack=sum(sout,2)./CMPs{cmp}.fold;
stack(:,cmp)=sum(sout,2)./CMPs{cmp}.fold;
%    CMPs{cmp}.stack=sum(sout,2);
%    stack(:,cmp)=sum(sout,2);

% No NMOR
%CMPs{cmp}.stack=sum(filt,2)./CMPs{cmp}.fold;
%stack(:,cmp)=sum(filt,2)./CMPs{cmp}.fold;

CMPs{cmp}.filt=filt;
%
% Plot the Result
if (figplot == 1)
   figure;
   colormap(gray)

   subplot(3,2,1)
   pcolor(P,T,A./max(A)); shading flat; set(gca, 'YDir', 'reverse' );
   caxis([-1 1]); ylim(ylimit);
   xlabel('Offset (m)'); ylabel('Time (s)');title('Raw data CMP');

   subplot(3,2,2)
```

```
        plot(sum(A,2),T)
        set(gca, 'YDir', 'reverse' )
        ylim(ylimit);xlabel('Amplitude'); ylabel('Time (s)');title('Stack');

        subplot(3,2,3)
        pcolor(P,T,filt./max(filt)); shading flat; set(gca, 'YDir', 'reverse' );
        caxis([-1 1]);ylim(ylimit)
        xlabel('Offset (m)'); ylabel('Time (s)');title('Processed data');

        subplot(3,2,4)
        plot(sum(filt,2),T);set(gca, 'YDir', 'reverse' );ylim(ylimit)
        xlabel('Amplitude'); ylabel('Time (s)');

        subplot(3,2,5)
        pcolor(P,T,sout./max(sout)); shading flat; set(gca, 'YDir', 'reverse' );
        caxis([-1 1]);ylim(ylimit);xlabel('Offset (m)'); ylabel('Time (s)');
        title('NMO Corrected data');

        subplot(3,2,6)
        plot(sum(sout,2),T)
        set(gca, 'YDir', 'reverse' );ylim(ylimit);xlabel('Amplitude'); ylabel('Time (s)');
    end
  %--------------------------------------------------------------------------
%%
  cmp
size(CMPs,2)
end

%% CMP Stack using Crewes Step 1

filtf1 = [90, 100]; % frequency filter bandpass WAS 50 60
filtf2 = [200, 210];
filtk1 = [-0.025 -0.035]; % fk filter bandpass
filtk2 = [0.025 0.035];
fk_va1 = 300; % minumum apparent velocity defining the rejection fan.
fk_va2 = 4000; % maximum apparent velocity defining the rejection fan va2>va1.
dv  = 100; % with of the taper on the edge of the rejection fan in velocityunits
```

```
cr = []; % Make a structure for the Crewes analysis

% For single component data
comps=(3:3:size(CMPdata.traces,1)); % Select the component
comp =3:3:size(data{1}.trace,2);

% Get the Time Vectors
cr.t        = CMPdata.T(1,:);     % Time Vector(s)

% Create the data matrix and apply any pre-stack processes
for i = 1:length(data)
   i
   length(data)
   cr.xrec{1,i}   = data{i}.X(comp);
   cr.xshots(i)   = data{i}.srcloc;
   cr.dist{1,i}   = data{i}.D(comp);

   % Get the Amplitudes
   filt = data{i}.trace(:,comp);

   % Apply a Bandpass Filter
   filt = filtf(filt,cr.t, filtf1, filtf2);

   % Assign to the data matrix
   cr.shots{1,i}  = filt;

end


%% Velocity Analysis Step 2

cr.spacing = (data{1}.x2 - data{1}.x1)/(data{1}.nrecs-1);
cr.cmpstart = min(CMPdata.M)-5;
cr.cmpend   = max(CMPdata.M)+5;

% Set the CMP Parameters
```

```
cr.cmp      = [cr.spacing cr.cmpstart cr.cmpend];          % CMP interval (m), Start (m) and End (m) of the CMP - make sure this spans the full space (if a CMP falls outside of your region it will produce an error)
cr.xv       = linspace(cr.cmpstart,cr.cmpend,floor(cr.cmpend-cr.cmpstart)+1); % Use a space that is 0,1000 every meter
cr.velocity = 850;                    % RMS Velocity (m/s)
cr.velrms   = ones(length(cr.t),length(cr.xv)).*cr.velocity; % Velocity grid


%% CMP and NMOR Corrections and plot Step 3
[cr.stack,cr.xcmp,cr.stackfold,cr.gathers,cr.xoffs]=cmpstack(cr.shots,cr.t,cr.xrec,cr.xshots,cr.cmp,cr.velrms,cr.t,cr.xv);

% Plot the resulting NMO corrections
figure;
plotimage(cr.stack,cr.t,cr.xcmp)

%% Plot stack

stack_f=stack;
tcor = 0.000; % Time correction (based on peak pick on P)
migv=800;

miglength=50; % Scale of features to be migrated (here in m)
maxdipang=30; % Maximum dip angle to migrate to

vals=(cr.t>=0); % Only migrate times that occur later than zero.
% Kirchoff migration
[seismig,tmig,xmig]=kirk_mig(cr.stack(vals,:),migv,cr.t(vals),cr.xcmp,[miglength 0.05*miglength 1 maxdipang 0.15*maxdipang 1]);

% Time window
ylimit=[min(cr.t)-tcor max(cr.t)-tcor];

cpt='gray';



figure;
```

```
% Plot the Migrated Result
%subplot(1,7,4:6);
imagesc(xmig,tmig-tcor,seismig); hold on;
colormap(cpt);
xlabel('Distance Along Seismic Line (m)'); ylabel('Two Way Travel Time (s)'); title(['2-D Reflectivity Structure on Nodal Line 1B']);
ylim(ylimit);
ylim([0 0.5]);

figure;
imagesc(midpts,T-tcor,envelope(stack_f));
colormap(turbo);
caxis([0 0.0053]);
xlabel('Distance Along Seismic Line (m)'); ylabel('Two Way Travel Time (s)'); title(['2-D Energy Envelope on Nodal Line 1A']);
%title('Raw Zero Offset Stacks');
%ylim(ylimit);
ylim([0 0.5]);
%%

%$$$$$$$$$$$$$$$$$$$$$$$$$$$$$$$$$$$$$$$$$$$$$$$$$$$$$$$$$$$$$$$$$$$$$$$$
% ALL CODE BLCOKS BELOW THIS POINT ARE FOR MAKING FIGURES FOR PAPER
%$$$$$$$$$$$$$$$$$$$$$$$$$$$$$$$$$$$$$$$$$$$$$$$$$$$$$$$$$$$$$$$$$$$$$$$$

%%%%%%%%%%%%%%%%%%%%%%%%%%%%%%%%%%%%%%%%%%%%%%%%%%%%%%%%%
%%%%%%%%%%%%%%%%%%%%%%%%%%%%


%% For Spectral Analysis by Shot Gather - FIGURE 6 A&B
[B,I]=sort(cr.dist{1,i}); % Sort into distance alignment

jj=100; % Shot number

filt = cr.shots{1,jj}(:,I);

pwspec  = [];
```

```
Fs = 2000;

pwspecall = [];
freqs = [];

for i = 1:size(filt,2)
    [pwspec(i).pxx,pwspec(i).f]=pwelch(filt(:,i),[],[],[],Fs,'psd'); % Gives the welch power spectral density

    pwspecall  = [pwspecall, pwspec(i).pxx];
    freqs      = [freqs; pwspec(i).f];

end

figure;

S=reshape(pwspecall,[513,51]);

%subplot(1,2,1)
pcolor(1:1:51,pwspec(1).f,10*log10(conj(S).*S));
shading flat
set(gca, 'YScale', 'log')

xlabel('Station #');
ylabel('Frequency (Hz)');

figure;
%subplot(1,2,2)

loglog(S,'-k');

xlabel('Frequency (Hz)');
ylabel('Power (dB)');

%%%%%%%%%%%%%%%%%%%%%%%%%%%%%%%%%%%%%%%%%%%%%%%%%%%%%%%%%%%%%%%%%%%%%%%%%%%%%%%%%%%%%%%%

%% For making the Amplitude vs Increasing Distance graph – FIGURE 13
```

```
aaxis = linspace(0,1,100);
aaxis(1,1) = 10^-4;
daxis = linspace(0,200,100);
a0=1;
frequency = 100;
c = 800;
Q = 3;
figure; hold on;
for i =1:6
    amplitude = a0.*exp((-1*frequency*daxis)/(c*Q));

     plot(daxis, amplitude,'k')

    Q = 3+i*2;

end
amplitude = a0.*exp((-1*frequency*daxis)/(c*20.5));
  plot(daxis, amplitude,'k');

x = linspace(160,160,100);
plot(x,aaxis,'LineWidth', 2, 'color', 'k');
x = linspace(80,80,100);
plot(x,aaxis,'LineWidth', 2, 'color', 'k');
ylim([10^-4 1]);
xlim([0 200]);
xlabel('Ray Path Distance (m)');
ylabel('Amplitude Decay (A/Ao)')
box on;
%%%%%%%%%%%%%%%%%%%%%%%%%%%%%%%%%%%%%%%%%%%%%%%%%%%%%%%%%%%%
%%%%%%%%%%%%%%%%%%%%%%%%%%%%



%% Amplitude Ratio vs Quality Factor Graph – FIGURE 14
Q1 = linspace(0,100,101);
frequency = 100;
```

```
figure;
plot(Q1,Aratio,'LineWidth', 2,'color','k');
hold on;
plot(Q1,Aratio2,'k');

xlim([0 30]);
ylim([0 10^1]);
xlabel('Quality Factor (Q)');
ylabel('Relative Amplitude (A_1/A_2)');


averatio = 4.71654
averatio2 = 2.88976
avevec = linspace(averatio, averatio, 101);
hold on;


plot(linspace(20.2,20.2,101),linspace(10^-3,10^3,101),'k--'); %QF line
plot(20.2,averatio,'ro','MarkerSize',3,'MarkerFaceColor','r'); %line 1a

plot(20.2,averatio2,'bo','MarkerSize',3,'MarkerFaceColor','b'); %line 1b

err = 0.04006;
err2 = 0.04934;

errorbar(20.2,averatio,err,err,'r','LineWidth',2);
errorbar(20.2,averatio2,err2,err2,'b','LineWidth', 2);
plot(Q1, linspace(averatio,averatio,101),'r--');

plot(Q1, linspace(averatio2,averatio2,101),'b--');

ylim([1 10]);
legend('\Delta x = 80 m (Line 1A)','\Delta x = 55 m (Line 1B)','Observed Q = 20.2','A_1/A_2 = 4.71654 (Line
1A)','A_1/A_2 = 2.88976 (Line 1B)','Location','northeast');
```